Atmos. Chem. Phys., 8, 4997–5016, 2008
www.atmos-chem-phys.net/8/4997/2008/

Atmospheric Chemistry and Physics

Laboratory studies of H_2SO_4/H_2O binary homogeneous nucleation from the SO_2+OH reaction: evaluation of the experimental setup and preliminary results

L. H. Young[1,*], D. R. Benson[1], F. R. Kameel[1], J. R. Pierce[2], H. Junninen[3], M. Kulmala[3], and S.-H. Lee[1]

[1]Kent State University, Department of Chemistry, Kent, OH, USA
[2]NASA Goddard Space Flight Center, MD, USA
[3]University of Helsinki, Department of Physical Sciences, Helsinki, Finland
[*]now at: China Medical University, Department of Occupational Safety and Health, Taichung, Taiwan

Received: 26 February 2008 – Published in Atmos. Chem. Phys. Discuss.: 9 April 2008
Revised: 15 July 2008 – Accepted: 6 August 2008 – Published: 28 August 2008

Abstract. Binary homogeneous nucleation (BHN) of sulphuric acid and water (H_2SO_4/H_2O) is one of the most important atmospheric nucleation processes, but laboratory observations of this nucleation process are very limited and there are also large discrepancies between different laboratory studies. The difficulties associated with these experiments include wall loss of H_2SO_4 and uncertainties in estimation of H_2SO_4 concentration ($[H_2SO_4]$) involved in nucleation. We have developed a new laboratory nucleation setup to study H_2SO_4/H_2O BHN kinetics and provide relatively constrained $[H_2SO_4]$ needed for nucleation. H_2SO_4 is produced from the SO_2+OH→HSO_3 reaction and OH radicals are produced from water vapor UV absorption. The residual $[H_2SO_4]$ were measured at the end of the nucleation reactor with a chemical ionization mass spectrometer (CIMS). Wall loss factors (WLFs) of H_2SO_4 were estimated by assuming that wall loss is diffusion limited and these calculated WLFs were in good agreement with simultaneous measurements of the initial and residual $[H_2SO_4]$ with two CIMSs. The nucleation zone was estimated from numerical simulations based on the measured aerosol sizes (particle diameter, D_p) and $[H_2SO_4]$. The measured BHN rates (J) ranged from 0.01–220 $cm^{-3}\,s^{-1}$ at the initial and residual $[H_2SO_4]$ from 10^8–10^{10} cm^{-3}, a temperature of 288 K and relative humidity (RH) from 11–23%; J increased with increasing $[H_2SO_4]$ and RH. J also showed a power dependence on $[H_2SO_4]$ with the exponential power of 3–8. These power dependences are consistent with other laboratory studies under similar $[H_2SO_4]$ and RH, but different from atmospheric field observations which showed that particle number concentrations are often linearly dependent on $[H_2SO_4]$. These results, together with a higher $[H_2SO_4]$ threshold (10^8–10^9 cm^{-3}) needed to produce the unit J measured from the laboratory studies compared to the atmospheric conditions (10^6–10^7 cm^{-3}), imply that H_2SO_4/H_2O BHN alone is insufficient to explain atmospheric aerosol formation and growth. Particle growth rates estimated from the measured aerosol size distributions, residence times (t_r), and $[H_2SO_4]$ were 100–500 $nm\,h^{-1}$, much higher than those seen from atmospheric field observations, because of the higher $[H_2SO_4]$ used in our study.

Correspondence to: S.-H. Lee
(slee19@kent.edu)

1 Introduction

Atmospheric particles affect atmospheric composition, cloud formation, global radiation budget, and human health. Nucleation is a gas-to-particle conversion process in which new particles form directly from gas phase species (Seinfeld and Pandis, 1997) and is a key process that controls particle number concentrations. Field studies have shown that new particle formation occurs ubiquitously in the atmosphere, ranging from ground-level rural and urban areas to the upper troposphere and lower stratosphere (Kulmala et al., 2004). The most common feature of the new particle formation events is a substantial increase of number concentrations of nucleation mode particles (diameter <20 nm), reaching up to 10^5–10^6 cm^{-3} in the condensable vapor-laden air. The involvement of sulphuric acid (H_2SO_4) in nucleation has been widely suggested, with the binary (Vehkamäki et al., 2002; Yu, 2006), ternary (Korhonen et al., 1999; Napari et al., 2002), or ion-induced nucleation (Yu et al., 1998; Lee et al., 2003; Lovejoy et al., 2004). However, it was often found

Table 1. A summary of previous laboratory studies of H_2SO_4–H_2O BHN, along with two studies from our group (including Benson et al., 2008). $n_{H_2SO_4}$ indicates the number of H_2SO_4 in the critical clusters, n_{H_2O} the number of H_2O molecules in the critical clusters, CIMS chemical ionization mass spectrometry, t_r flow residence time, t_n nucleation time, WLF Wall Loss Factor of H_2SO_4, RSD the relative standard deviation, and R1 the $SO_2 + OH \rightarrow HSO_3$ reaction.

Reference	H_2SO_4Production	H_2SO_4 Measurements	$[H_2SO_4]$ (cm^{-3})	RH (%)	$J(cm^{-3}s^{-1})$	$n_{H_2SO_4}$; n_{H_2O}	t_r; t_n(s)	WLF	Stability Experiments
Wyslouzil et al., 1991a	Liquid H_2SO_4	Mass balance calculation (initial conc.)	1.3×10^{10} to 1.5×10^{11} (initial conc.)	0.6–65	0.001–300	4–30; 9	18; –		Ran experiments for at least 10 h; allowed 2 to 5 min for stabilization of new conditions
Viisanen et al., 1997	Liquid H_2SO_4	Mass balance calculation (initial and residual conc.)	1×10^{10} to 3×10^{10} (initial conc.)	38 and 52	2–3000	21 and 10; –	117; 50	1.9	Stabilized all temperatures and humidities before measurements; stable operation of at least 1 h with RSD<10%
Ball et al., 1999	Liquid H_2SO_4	CIMS (measured residual and calculated initial conc.)	2.5×10^{9} to 1.2×10^{10} (residual conc.)	2–15	0.01–1000	7–13; 4–6	26; 4	22	Initialized new experimental conditions overnight
Berndt et al., 2005, 2006	R1	Organic titration reactions and kinetic model calculation (residual conc.)	1×10^{7} to 1×10^{8} (residual conc.)	11–60	0.1–100 000	4–6; -	>290; –		
Zhang et al., 2004	Liquid H_2SO_4	CIMS (residual conc.)	4×10^{9} to 1×10^{10} (residual conc.)	5	0.3–500		7–12; –		
Benson et al., 2008	R1	CIMS (measured residual and calculated initial conc.)	3×10^{6} to 2×10^{9} (residual conc.)	11–50	0.1–10 000	2–10; 10–15	20–77; 10–38	2.6–29.9	Ran setup for 15 min; used the first 10 min for data analysis
This study	R1	CIMS (measured residual and calculated initial conc.)	1×10^{8} to 1×10^{10} (residual conc.)	11–23	0.01–220	3–8; –	5–54; 3–27	1.3–12	Ran set up for 15 min; but for J calculations, initial N were corrected with a factor of 5 to convert them to the steady state concentrations

that the nucleation rate (J) predicted from nucleation theories cannot explain the atmospheric observations (e.g., Weber et al., 1996). The current nucleation theories also contain high uncertainties over many orders of magnitude, because these theories are not fully tested and constrained by laboratory observations. Recently, Kulmala et al. (2007a) showed direct evidence of aerosol nucleation by measuring neutral clusters and small aerosol particles at the 1.5 nm size range in the boreal forest atmosphere and suggested that their findings support the cluster activation theory of atmospheric aerosol nucleation proposed by Kulmala et al. (2006).

Heist and He (1994) and Laaksonen et al. (1995)'s review papers discuss nucleation measurements from earlier studies. Table 1 summarizes more recent H_2SO_4/H_2O binary homogeneous nucleation (BHN) laboratory studies found in the literature. At present, not only is the number of laboratory studies of H_2SO_4/H_2O BHN limited, but also there are large discrepancies in J and the $[H_2SO_4]$ involved in nucleation reported from different studies. There are several important aspects in laboratory H_2SO_4 nucleation experiments, such as the method used to produce H_2SO_4 vapor, estimation of $[H_2SO_4]$ used for nucleation, wall loss of H_2SO_4 in the nucleation reactor, estimation of the nucleation region, and the stability of the nucleation system especially with regard to particle measurements. These factors directly contribute to the uncertainties in J and the $[H_2SO_4]$ required for nucleation.

Several laboratory studies produced H_2SO_4 vapors by saturating a carrier gas with the vapor from a liquid pool or vaporizing the H_2SO_4 acid liquid at high temperatures for simplicity and calculating the saturation ratio, relative acidity, or the H_2SO_4 concentration ($[H_2SO_4]$) based on mass balance (Reiss et al., 1976; Mirabel and Clavelin, 1978; Wyslouzil et al., 1991a; Viisanen et al., 1997). These experiments were also often made in continuous-flow reactor systems. For example, Wyslouzil et al. (1991) investigated the H_2SO_4, relative humidity (RH), and temperature dependence of J. At relative humidity (RH) between 0.6 to 65% and temperatures of 293, 298, and 303 K, they measured J between ~0.001 to ~300 $cm^{-3}\,s^{-1}$ for calculated relative acidities between 0.04–0.46; the estimated numbers of H_2SO_4 molecules in the critical clusters ($n_{H_2SO_4}$) ranged from 4–30. Viisanen et al. (1997) measured J between 2–3000 $cm^{-3}\,s^{-1}$ for calculated $[H_2SO_4]$ between 1×10^{10} to 3×10^{10} cm^{-3} at 298 K and ambient pressure; the estimated numbers of H_2SO_4 molecules in the critical clusters were 21 and 10 at RH of 38% and 52%, respectively. Ball et al. (1999) directly measured $[H_2SO_4]$ with a chemical ionization mass spectrometer (CIMS) and obtained J ranging from approximately 0.01–1000 $cm^{-3}\,s^{-1}$ for residual $[H_2SO_4]$ between ~2.5×10^{9} to 1.2×10^{10} cm^{-3} at RH from 2–15%, 295 K and ambient pressure. The estimated $n_{H_2SO_4}$ and the numbers of H_2O molecules in the critical clusters (n_{H2O}) ranged from 7–13 and from 4–6, respectively (Ball et al., 1999). With a similar approach with CIMS, Zhang et al. (2004) obtained J ranging from ~0.3–500 $cm^{-3}\,s^{-1}$ for residual $[H_2SO_4]$ from ~4×10^{9} to 1.0×10^{10} cm^{-3} at RH of ~5%, 298 K and ambient pressure.

Reiss et al. (1976) and Boulaud et al. (1977) have noted the difficulties associated with liquid H_2SO_4 samples; for

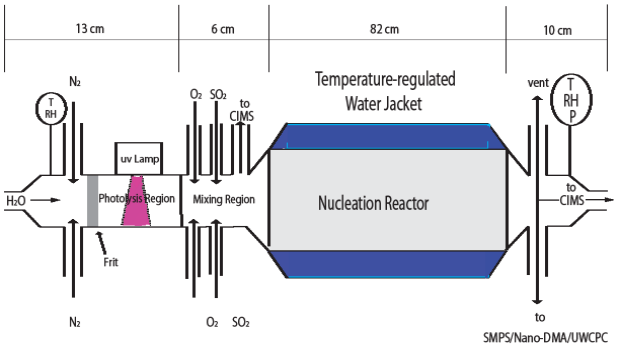

Fig. 1. A schematic of the Kent State University nucleation experimental set-up that consists of OH photolysis cell, a fast flow reactor for nucleation of H_2SO_4/H_2O, a SMPS/UWCPC system for particle measurements, and a CIMS for the residual H_2SO_4 detection at the end of the nucleation reactor. Note this is the system used for most of the results shown in the present study, but we also performed additional experiments with two CIMSs to measure both the initial and the residual [H_2SO_4] to verify WLF calculations (Fig. 4). For the experiments with two CIMSs, the 2nd CIMS inlet was connected to the position after the SO_2 introduction and before the nucleation region. Nucleation zone was estimated to be about 40 cm (Sect. 3.3).

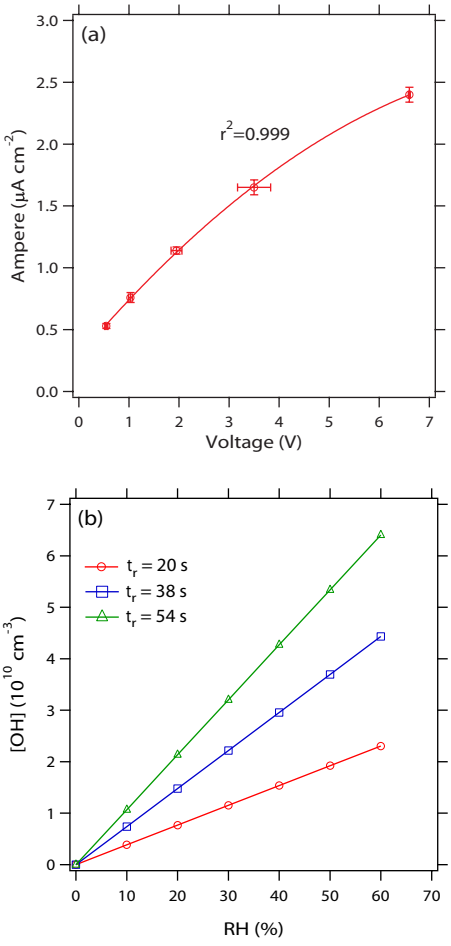

Fig. 2. (a) Calibration curve of photon intensities measured in voltage by a Hamamatsu phototube and those in ampere by a NIST-certified photodiode. Error bars indicate one standard deviation around the mean. **(b)** The calculated [OH] produced from water vapor UV absorption as a function of RH (Sect. 2.1). Since under typical experimental conditions [SO_2]≫[OH], the initial [H_2SO_4]=[OH]; these two values were in fact nearly on the same order, within experimental uncertainties (Fig. 6, Table 2).

example, the corrosiveness and extremely low vapor pressure of H_2SO_4, and the vapor equilibrium in the carrier gas and the homogeneity of the H_2SO_4/H_2O mixture are difficult to characterize. There are also other studies that have produced H_2SO_4 from gas phase SO_2 by means of α-ray irradiation for ion-induced nucleation studies (Diamond et al., 1985; Mäkelä et al., 1995; Kim et al., 1997). Christensen et al. (1994) used photolytic excitation of SO_2 (wavelength between 240 and 330 nm) in an $SO_2/NH_3/H_2O$ ternary system to produce H_2SO_4. Boulaud et al. (1977) used in-situ gas phase reaction of SO_3+H_2O for the production of H_2SO_4 vapors, and obtained J of $1\,cm^{-3}\,s^{-1}$ for [H_2SO_4] from 10^{10} to $10^{11}\,cm^{-3}$ at RH from 15–70% and 293 K. Berndt et al. (2005, 2006) used the gas phase reaction of SO_2 + OH to produce H_2SO_4 vapor, via the following reactions:

$$SO_2 + OH \rightarrow HSO_3 \text{ (Rate limiting step)} \quad \text{(R1)}$$

$$HSO_3 + O_2 \rightarrow SO_3 + HO_2 \quad \text{(R2)}$$

$$SO_3 + 2H_2O \rightarrow H_2SO_4 + H_2O \quad \text{(R3)}$$

They calculated [H_2SO_4] from the estimated [OH] and [SO_2]; [OH] was calculated from titration reactions of hydrocarbons and OH. From this method, they obtained a low threshold of [H_2SO_4] needed for nucleation, 10^6–$10^7\,cm^{-3}$, considerably lower than those from other previous laboratory nucleation studies (Viisanen et al., 1997; Ball et al., 1999; Zhang et al., 2004). Recent studies also suggested a new pathway to produce particles from SO_2 and OH other than through R1–R3, involving formation of gas phase HSO_5 that may contribute to new particle formation (Berndt et al., 2008; Stratmann et al., 2008).

Wall loss of H_2SO_4 is one of the challenges in nucleation experiments. Some studies provided initial [H_2SO_4] (Wyslouzil et al., 1991a; Viisanen et al., 1997), whereas others provided only the residual [H_2SO_4] (Berndt et al., 2005, 2006; Zhang et al., 2004). Ball et al. (1999) corrected the residual [H_2SO_4] with WLFs to estimate the initial [H_2SO_4]. Ball et al. (1999) estimated a factor of 2 loss of H_2SO_4 in the "nucleation zone" in their fast flow reactor (corresponding to t_n of 4 s; the t_r in the entire flow reactor was ∼26 s) (I.D.=4.9 cm). By further including other additional factors, such as losses on several joints inside the nucleation reactor,

Ball et al. (1999) have reported an overall WLF of 22. Viisanen et al. (1997) have estimated WLF of H_2SO_4 of 1.7 for nucleation time (t_n) of 50 s from their H_2SO_4–H_2O nucleation experiments in which a laminar flow diffusion chamber (I.D.=2.4 cm) was used as the nucleation reactor.

Nucleation zone and particle stability were also addressed by different investigators. So far, Ball et al. (1999) have provided the most comprehensive information on "nucleation zone" using a movable tube to measure particle number concentrations (N) as a function of axial position of the nucleation reactor; they estimated t_n of 4 s while the total t_r was 26 s. In Ball et al. (1999), gases were left flowing to maintain cleanness and left overnight under the initial experimental conditions for the next day's experiments to achieve stable experimental conditions. To achieve the steady state of nucleation, Wyslouzil et al. (1991a, b) have run experiments for several days before starting experiments to get reproducible data. Similar approach was also applied in Viisanen et al. (1997), who also evaluated if their system was stable or not with the relative standard deviation of the measured N less than 0.10 for a period of at least an hour.

We have performed laboratory studies of H_2SO_4/H_2O binary homogeneous nucleation in a fast flow reactor at 288 K, RH from 11 to 23%, and ambient pressure. Our laboratory system is constructed based on the selective combination of the experimental methods utilized in Berndt et al. (2005, 2006), Ball et al. (1999) and Zhang et al. (2004). Similarly to Berndt et al. (2005, 2006), we also used R1–R3 to in-situ produce H_2SO_4; but we measure the residual [H_2SO_4] directly with a CIMS, the same method utilized as in Ball et al. (1999) and Zhang et al. (2004). Unlike Berndt et al. (2005, 2006) where OH forms from ozone UV reactions, in the present study OH is produced by water photolysis to allow direct measurement of [OH]. We have also calculated WLFs of H_2SO_4 as a function of t_r by assuming that H_2SO_4 wall loss is diffusion limited (Hanson and Eisele, 2000); using simultaneous measurements of the initial and residual [H_2SO_4] with two CIMSs, we further verified these calculated WLFs. The nucleation zone was estimated from numerical simulations using the measured aerosol size distributions, the residual [H_2SO_4] and the estimated WLFs. Stability experiments were also performed in order to provide reproducible N and J. The primary objectives of this study are to evaluate the performance of the nucleation experimental setup from the measured J at various [H_2SO_4], RH and t_r conditions and provide relatively constrained [H_2SO_4] needed for H_2SO_4/H_2O BHN. Additional kinetics results from our laboratory studies are also shown in Benson et al. (2008) (summarized in Table 1).

2 Experimental setup

Our nucleation experimental setup consists of (a) an OH generator, (b) a temperature- and RH-controlled, fast flow nucleation reactor, (c) a high sensitivity, atmospheric-pressure CIMS to measure low concentrations of H_2SO_4, and (d) TSI aerosol spectrometers to measure D_p and N (Fig. 1). Table 2 shows the typical experimental conditions and a summary of the results shown in the present study. Most of the experiments were performed with one CIMS located at the end of the nucleation reactor to measure residual [H_2SO_4], and the initial [H_2SO_4] were estimated with the residual [H_2SO_4] and WLFs (Table 2). Independently, initial [H_2SO_4] were also estimated from the [OH] produced from water UV absorption ([SO_2]$\gg$[OH] under the typical experimental conditions) and as shown in Table 2, the [OH] values were in good agreement with the initial [H_2SO_4] estimated from WLFs, if the reactions of OH and possible CO impurities in the system were taken into account (Table 2). There were also additional experiments made with two CIMSs to simultaneously measure the initial and the residual [H_2SO_4]; these measurements proved that the calculated WLFs from the diffusion limited method are indeed valid (Sect. 3.1).

2.1 OH radicals and H_2SO_4 vapor generation

H_2SO_4 vapor is produced in-situ via R1–R3. SO_2 was taken from standard SO_2 gases (1 and 100 ppmv) that were further diluted with standard air. OH forms from the photodissociation of H_2O vapor in a quartz tube (13 cm long with 2.54 cm I.D.), using a mercury lamp (Pen-Ray 11SC-1) filtered for λ<185 nm with a bandpass filter (Omega Optical XB32 185NB20). Both the lamp and the filter are housed inside a temperature-controlled metal box, which is purged with a constant N_2 flow rate to provide a stable photon flux. At the bottom of the box, there is a radiation exit slit with the long side parallel to the flow direction. The photon flux exiting the light source is detected as a function of distance using a solar-blind CsI phototube (Hamamatsu R5764), calibrated against a (National Institute of Standard Technology) NIST-certified Si photodiode (40599S). The photocurrents were measured with a pico-ampere meter (Keithley 6517A) or converted to voltage signals with resistors and measured by a voltage meter (Fig. 2a). By measuring H_2O mixing ratios and UV photon intensities, [OH] is calculated based on the known photochemical reaction rates (absolute calibration) (Cantrell et al., 1997). The photon flux, I, at radiation wavelength, λ (nm), is determined by:

$$I(\lambda) = \frac{A(\lambda)}{e \times \varepsilon(\lambda)} \quad (1)$$

where A is the measured ampere at λ, e is the electronic charge (1.6×10^{-19}C), and ε is the quantum efficiency of the

Table 2. Experimental conditions and the results shown in the present study. Wall loss factors (WLFs) were calculated by assuming that wall loss is diffusion-limited (Sect. 3.1). The initial $[H_2SO_4]$ were estimated from the WLFs, the CIMS-measured $[H_2SO_4]$ and the calculated $[H_2SO_4]$ in the particle phase (Sect. 3.2). [OH] calculated from water vapor UV absorption are also shown for comparison. Also see Fig. 6 for the evolution of gas phase species as a function of time in the nucleation reactor.

Data Used	RH (%)	Particle Mode	SO_2 Source (ppmv)	Q_{total} (lpm)	Q_{SO2} (lpm)	Reactor ID; Length (cm)	t_r (s)	[OH] Calculated from H_2O Photolysis (10^9 cm^{-3})	$[SO_2]$ (10^{13} cm^{-3})	WLF	$[H_2SO_4]_0$ Calculated from WLF (10^9 cm^{-3})	$[H_2SO_4]_{CIMS}$ (10^9 cm^{-3})	Part Conc. (cm^{-3})	J (cm^{-3}s^{-1})	$n_{H_2SO_4}$
Fig. 17(a): C; Fig. 14	11	CPC	100	5–5.2	0.08–0.2	5.08; 82	19–20	3.5–3.6	3.2–8.0	2.5–2.6	1.4–3.2	0.52–1.3	0.12–4	0.01—0.4	3–6
Fig. 17(a): B; Figs. 9 and 14	15	CPC	100	5–5.2	0.08–0.2	5.08; 82	19–20	4.8–5.0	3.1–8.0	2.4–2.5	3.1–9.6	1.3–3.9	0.08–34	0.01–3.4	7
Fig. 17(a): D; Fig. 10	15	CPC	1	5	0.30–0.9	2.54; 80	5	5.0	0.12–0.36	1.3	0.40–0.72	0.32–0.58	0.27–2.1	0.11–0.8	4–5
Fig. 17(a): E; Figs. 9 und 10	15	CPC	1	5.2	0.10–0.75	5.08; 82	19	4.8	0.038–0.29	2.4	0.21–0.58	0.09–0.24	0.13–12	0.01–1.2	5–8
Fig. 17(a): A; Fig. 14	23	CPC	100	5	0.01–0.2	5.08; 82	19	8.8	0.4–8	2.4	2.1–23	0.87–9.6	$0.6–2.1\times10^3$	0.06–220	3
Figs. 11(a), 12(a), 13	23	SMPS	100	4.1	0.12–0.2	5.08; 82	24	11	5.9–9.8	3.0	4.5–7.2	1.5–2.4	$220–6.9\times10^3$	–	–
Figs. 11(b), 12(b), 13	23	SMPS	100	2.6	0.12–0.2	5.08; 82	37	17	9.2–15	5.4	7.4–8.4	1.4–1.5	$1.4\times10^4 – 1.3\times10^5$	–	–
Figs. 11(c), 12(c), 13	23	SMPS	100	1.8	0.08–0.2	5.08; 82	54	24	8.9–22	12	1.2–1.5	0.10–0.12	$1.4\times10^4 – 5.5\times10^5$	–	–

NIST-certified photodiode at λ. [OH] then is calculated from the following equations (Cantrell et al., 1997):

$$[OH] = J_{H_2O}[H_2O]t_p \quad (2)$$

$$J_{H_2O} = I\sigma\phi \quad (3)$$

where J_{H_2O} is the H_2O photolysis rate, σ the absorption cross-section of water vapor (σ=7.14×10^{-20} cm^2 molecule^{-1} Cantrell et al., 1997), ϕ the quantum yield (ϕ(OH)=1.0 DeMore et al., 1997), and t_p the photolysis time. $[H_2O]$ was determined from the measured temperature and RH (%):

$$[H_2O] = \frac{RH}{100}\frac{p_s}{p_t}N_d \quad (4)$$

where p_s is the H_2O saturation vapor pressure [e.g., 1612 Pa (or 12.09 torr) at 288 K (NIST, 2005)], p_t the total pressure, and N_d the number concentration of dry air molecules. At typical experimental conditions, A=1.2×10^{-5} A cm^{-2}, I=1.4×10^{14} photon cm^{-2} s^{-1}, and hence J_{H_2O}=9.7×10^{-6} s^{-1}. Thus, under these conditions, the [OH] produced were in the 10^9–10^{10} cm^{-3} range as a function of RH (Fig. 2b).

When $[SO_2]>>[OH]$ which is the case for our experimental conditions (Table 2), the initial $[H_2SO_4]$=[OH] based on R1. Thus this OH production method by water vapor UV absorption, as compared to ozone photolysis (utilized in Berndt et al., 2005, 2006), not only minimizes other chemical species (such as ozone) in the reactor, but also provides direct estimation of OH (and thus the initial $[H_2SO_4]$). As shown in Table 2, for the majority of our experiments, these [OH] values were usually slightly higher but within the same order as the initial $[H_2SO_4]$ calculated from the residual $[H_2SO_4]$ and WLFs (Sect. 3.1; an example is shown in Fig. 6). There were also a few cases where [OH] was up to one order of magnitude higher than the initial $[H_2SO_4]$. These differences were caused by uncertainties in the measurements of accurate photon flux (I) (and thus the H_2O photolysis rate J_{H_2O}) and $[H_2O]$, in addition to uncertainties associated with the initial $[H_2SO_4]$ estimation. Also, as will be shown in Sect. 3.2, OH radicals also react with other low concentrations of CO impurities (estimated to $<\sim$200 ppbv; Sect. 2.2) and some possible hydrocarbons (not estimated) that may exist in the reactor (not determined) and thus we expect that some of the produced OH radicals were consumed before R1. Regardless of these experimental uncertainties, such an agreement is remarkable, especially considering two entirely independent methods used in the [OH] and the initial $[H_2SO_4]$ estimations.

2.2 Nucleation reactor

The nucleation reactor is made of a fast-flow reactor (Pyrex cylinders with a length of 80 or 82 cm and with an inner diameter of 2.54 or 5.08 cm) with a laminar, fast flow. The reactor is also controlled for temperature with a refrigerating/heating circulating bath (Cole-Parmer Model 12101-31) and washed with distilled water daily to remove H_2SO_4 and particles deposited on its inside wall during the previous day's experiments. The total pressure in the nucleation reactor was $\sim$97.3 kPa (slightly higher than the room air pressure to prevent leak from the room air). The total flow rate (Q_{total}) was between 1.8–5.2 liter per minute (lpm) and t_r was estimated to be from 5–54 s. As will be shown in Sect. 3.3, nucleation zone was characterized to be about 40 cm and therefore, t_n=0.5 t_r.

The total flow was composed primarily of SO_2 and N_2. The SO_2 flow rate (Q_{SO_2}) varied between 0.01–0.9 lpm,

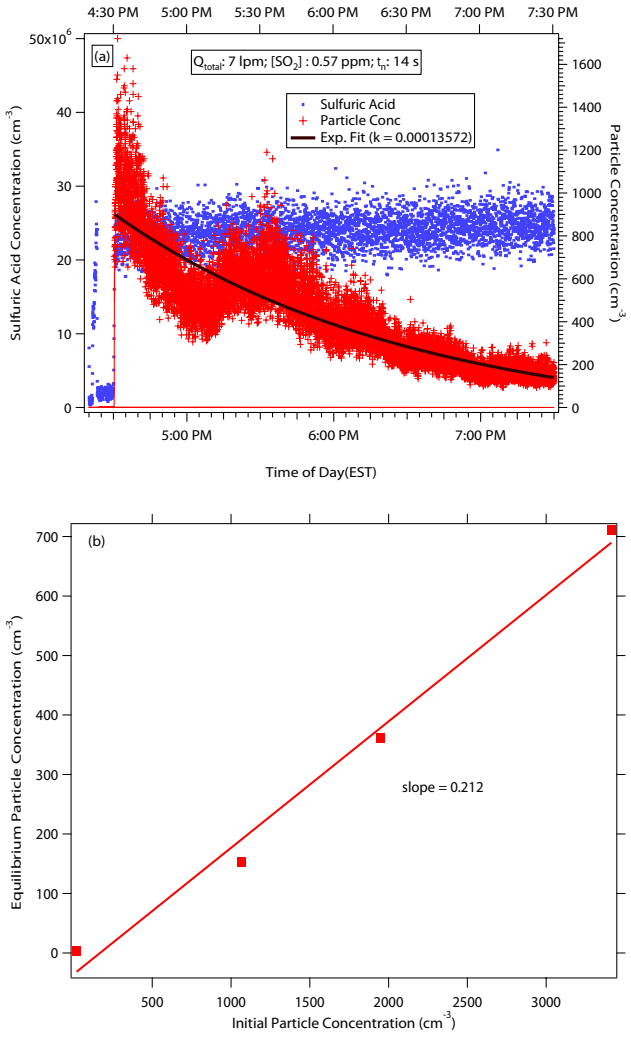

Fig. 3. **(a)** Stability experiments for residual [H_2SO_4] measured by CIMS (blue dots) and N measured by water-CPC (red crossings). The black line shows the fitting of an exponential decay and from this fitting, we also derived the first order loss rate of particles (1.4×10^{-4} s^{-1}). (2) The N measured by water-CPC after 3 h when the steady state (or equilibrium) has been reached vs. those measured within the initial first few minutes. This factor of 5 was taken into account for nucleation rates (J) shown in the present study.

depending on the SO_2 concentration of the cylinder. The dry N_2 flow rate was adjusted simultaneously with the Q_{SO_2} to maintain a constant Q_{total}. The H_2O flow (i.e., humidified N_2 flow) varied between 0.01 to 0.4 lpm to maintain the target RH values. The O_2 flow was maintained at 0.001 lpm regardless of the total flow rate. Only high purity standard gases (nitrogen, oxygen, and SO_2) (Linde Gas and Airgas Inc.) and distilled water were introduced in the nucleation region. The main flow of the nucleation reactor was nitrogen that is used to bubble water; nitrogen gases vaporized from liquid nitrogen were used to reduce ammonia impurities (<20 pptv) (Nowak et al., 2007). We have also used the silicon phosphates ammonia scrubber (Perma Pure Inc.) to test the effects of possible ammonia impurities in our system on the H_2SO_4–H_2O BHN experiments, and those effects were found negligible. Test results with CO scrubbers (Carus Carulite 300) also showed that CO impurities in the photolysis and nucleation reactor are not significant (<200 ppbv). The flows of these gases in the water photolysis cell, the nucleation reactor, and CIMS were controlled with seven high precision mass flow controllers (MKS). These mass flow controllers were also regularly calibrated with a standard flow meter (DryCal DC-2, Bio International Corp.).

The photolysis tube was exposed to indoor temperature (295±2 K), and the nucleation tube was maintained at 288±0.05 K with a refrigerating circulating bath (Cole-Parmer Model 12101-31). RH was controlled mainly by changing the flow rates of water vapor into the nucleation reactor. There are three sets of temperature and RH Campbell Scientific CS215), and pressure sensors (Granville-Phillips 275), in our nucleation reactor. The RH sensors are calibrated and NIST and National Physical Laboratory (NPL) traceable and have an accuracy of ±4% over RH from 0–100%; comparison results with several RH sensors with the laboratory room air and the air in the nucleation reactor showed a good agreement within this accuracy.

2.3 Particle measurements and stability

A nanoparticle differential mobility analyzer (Nano-DMA) (TSI 3080N) and an ultrafine water condensation particle counter (water-CPC) (TSI 3786) were used for particle number and size distribution measurements. These aerosol instruments were operated in two modes, the CPC standalone mode and the Nano-DMA/water-CPC combination mode. In the standalone mode, water-CPC has a 50% detection efficiency at ∼2.5 nm and gives total particle number concentrations every 5 s. The water-CPC inlet flow was set at 0.6 lpm. In the Nano-DMA/water-CPC combination mode, size-resolved particle number concentrations were obtained from 2.5–102 nm every 180 s. The SMPS inlet and sheath flows were set at 0.6 and 6 lpm, respectively. For J values shown in the present study, the N were determined using the water-CPC standalone mode, while SMPS combination mode was used to provide aerosol sizes.

We found that the measured N was generally not as stable as the H_2SO_4 measurements (Fig. 3). The stability tests show that it took a certain period of time (e.g., 3 h) for the N to reach a steady state. The general trend was that the N increased in the first few minutes, but after the initial increase N actually started to decrease for a certain period of time (Fig. 3a). The relative standard deviation of the N decreased with time, for example, 0.39 within the first 20 min and down to <0.10 after allowing the gases to run through the tube for several hours. The cause of such instability is not verified, but we suspect that the newly formed particles are

not uniformly distributed inside the wall. The effect of inhomogeneity seemed to be magnified when the measured number concentrations were on the order of 100 cm^{-3} or less. From the stability measurements, we estimated the first order loss rate of particles to be 1.4×10^{-4} s^{-1} (much smaller than that of H_2SO_4, 0.053 s^{-1}, as shown Sect. 3.1). Here, "initial" N is referred to as that measured at the end of the nucleation reactor within the first few minutes under a specific experimental condition, and "steady state" N to as that measured at the end of the nucleation reactor when the system becomes stabilized after several hours under the same experimental conditions. Very conveniently, however, there was a linear relationship between the initial N and the N after enough time (e.g., 3 h) has been allowed for the steady state to be reached; the initial N were usually 5 times higher than their steady state concentrations. It will be ideal to perform experiments after running the experiments for several hours under the same experimental conditions to make sure that steady state is achieved. However, the results shown in the present study were taken only within first several minutes and we used this correction factor of 5 (Fig. 3b) to calculate the steady state N. That is, the J values shown in the present study were derived from the steady state N, corrected from the initial N with this factor of 5.

The integrated "total" particle number concentrations from the combination mode were on average a factor of 5 or 10 lower than the total particle number concentrations from the standalone mode when sampling particles generated in the nucleation reactor. For higher N, this ratio was higher for a similar set of conditions. We also performed similar tests by sampling the laboratory room air. The N between the standalone mode and combination mode were more similar (standalone vs. combination = 1:0.66) when sampling laboratory room air than sampling from the nucleation reactor (standalone vs. combination = 1:0.1 or 1:0.2). Such differences between standalone and combination modes are in part because of the additional tubing length involved in the SMPS measurement in this study. Based on Baron and Willeke (2001), the estimated fractional penetration efficiency of 3 nm particles through the additional 39 cm long cylindrical tubing at 0.6 lpm is 0.65. In addition, it is possible that the CPC may be able to detect H_2SO_4 particles smaller than the stated minimum measurable size (~2.5 nm). When the CPC is operated with the nano-SMPS, some of the particles smaller than 2.5 nm may be excluded in the nano-DMA, hence further contributing to the concentration difference. Note that however Berndt et al. (2006) showed reasonable agreement between the combination and standalone mode.

The J values shown in the present study were measured only with water-CPC (TSI 3786). But we also made comparisons with water CPC and butanol-CPC (TSI 3776) and there was an almost linear relation between these two measurements when sampling the particles generated in the nucleation reactor, with the water-CPC concentrations about 8 times higher than the butanol-CPC concentrations. On the other hand, when sampling the laboratory room air, the concentrations measured from WCPC were only ~7% higher than those measured by the butanol-CPC. Since the particles generated in the nucleation reactor are presumably pure H_2SO_4 particles whereas the particles in the lab air are more mixed with H_2SO_4(or sulfate) and organic components, these results indicate that water can activate, and condense on, H_2SO_4 particles more effectively than butanol, consistent with Kulmala et al. (2007b).

The Jwere determined by the measured particle number concentrations (N) and t_n (t_n=0.5t_r as shown in Sect. 3.3). Because critical clusters (~1.5 nm) (Kulmala et al., 2007a) are typically smaller than the minimum measurable size of the CPC, the J reported here, theoretically, is not the actual J, but rather the formation rate of particles with diameters larger than ~2.5 nm, the so-called "apparent formation rate" (Kerminen and Kulmala, 2002). However, when coagulation growth is negligible, which was the case for most of our experiments, the values estimated from such a calculation are close to the actual J values (Kulmala et al., 2004).

The numbers of H_2SO_4 molecules ($n_{H_2SO_4}$) in the critical clusters are calculated with the J vs. [H_2SO_4] at specific values of RH and absolute temperature T, based on the first nucleation theorem (Kashchiev, 1982; Strey and Viisanen, 1993):

$$\left.\frac{\partial \ln J}{\partial \ln[a_1]}\right|_{a_2,T} \approx n_{H_2SO_4} \quad (5)$$

where a_1 and a_2 are the activity of species 1 and 2, respectively. In practice, the $n_{H_2SO_4}$ values for H_2SO_4 molecules can be approximated by fitting the data points with power regression:

$$J = c\,[H_2SO_4]^{n_{H_2SO_4}} \quad (6)$$

where c is a constant, at specific values of temperature and RH.

2.4 H_2SO_4 detection by CIMS

Our CIMS was built by Greg Huey's group at Georgia Tech based on Eisele and Tanner (1993). The CIMS instrument is constructed from an ion source, an ion molecular reactor, and a quadrupole mass spectrometer. The following ion molecule reaction

$$NO_3^- + H_2SO_4 \rightarrow HNO_3 + HSO_4^- \quad (R4)$$

is used to detect H_2SO_4 (Viggiano et al., 1997). This reaction scheme has been proven to be very effective for H_2SO_4 measurements, and this is one of the very few methods currently available to detect H_2SO_4 at atmospheric concentrations (Eisele and Tanner, 1993; Huey, 2007). This low detection limit is achieved because of its high reaction rate, high selectivity against other species, and the atmospheric pressure ionization used.

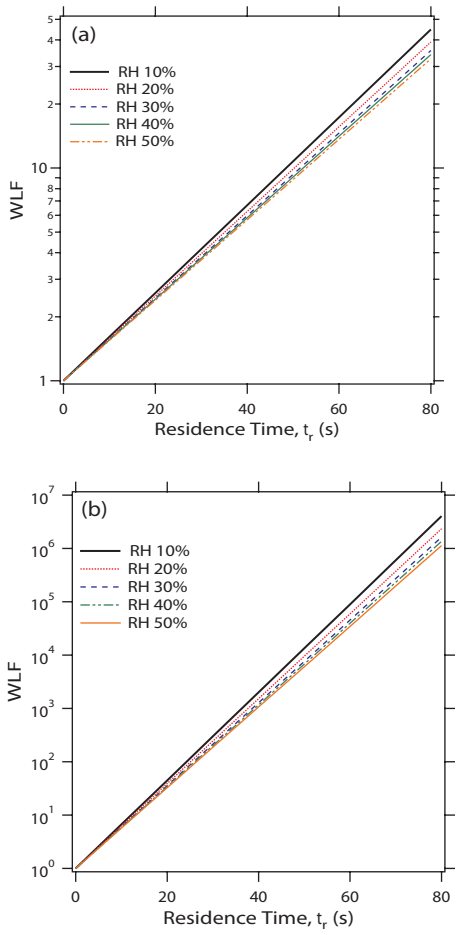

Fig. 4. The calculated WLFs as a function of t_r and RH for the nucleation reactor with I.D. of **(a)** 5.08 cm and **(b)** 2.54 cm. In these calculations, we assume that wall loss is a diffusion limited process based on Hanson and Eisele (2000) (Sect. 3.1) and experiments show that this assumption is valid (Fig. 5).

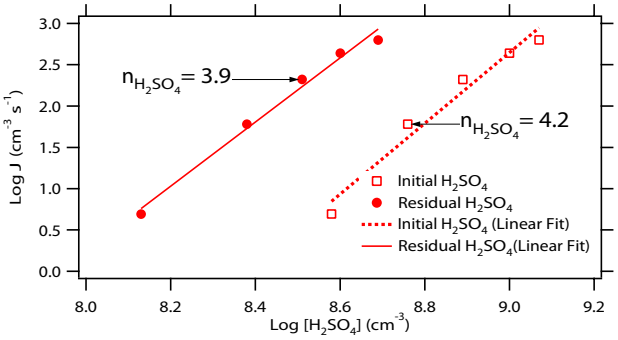

Fig. 5. The measured J as a function of the initial and residual $[H_2SO_4]$, measured simultaneously with two CIMSs. The conditions for this experiment were a total flow of 5 lpm (19 s t_r), an RH of 16%, and $[SO_2]$ ranging from 0.8 to 4 ppmv. Note, these two linear fittings have approximately the same slopes, indicating that wall loss of H_2SO_4 is a first order process – an assumption used in our WLF calculations (Sect. 3.1). Furthermore, the initial $[H_2SO_4]$ were about 2.5 times higher than the residual $[H_2SO_4]$, while the estimated WLF from diffusion limited method (Sect. 3.1) was similar to this value for the same t_r (Fig. 4b), showing that our WLF estimations are valid.

The ^{210}Po radiation source is used as an ion source. The ion source region also has a unique design to prevent artifact H_2SO_4 detection. Because OH radicals also form from water molecule dissociation reactions in the ion source region (^{210}Po radiation), there is a possibility that those OH radicals react immediately with the SO_2 in the air samples to produce H_2SO_4. To eliminate such artifacts of H_2SO_4 formation, a weak electric field is applied between the ion source region and the center of the sampling inlet so that only the electrically charged NO_3^- ions (not the neutral OH radicals) travel through to the center of the sampling inlet to react with H_2SO_4. In addition, C_3F_6 gases are also mixed with HNO_3 gases so that OH radicals are efficiently removed by C_3F_6. With the current CIMS configuration, the background $[H_2SO_4]$ is negligible even when high concentrations of SO_2 gases are introduced into the CIMS. A collision dissociation chamber (CDC) is applied to dissociate the weakly bonded ion molecule clusters of sulphuric acid, nitric acid, and water molecules by low energy collisions with N_2 molecules to provide simpler ion peaks. Ions are focused by an octopole before reaching the quadrupole mass filter (Extrel) and then detected by a channeltron detector (K+M). The pressures in the CDC, octopole, and quadrupole are about 10^1, 10^{-1}, and 10^{-3} Pa, respectively.

The $[H_2SO_4]$ was calculated from the ratio of the HSO_4^- to NO_3^- ion counts $[HSO_4^-]/[NO_3^-]$, the rate constant k of R1, and the reaction time t based on Huey (2007):

$$[H_2SO_4] \approx \frac{[HSO_4^-]}{[NO_3^-]} kt \quad (7)$$

Where k for R1 is 1×10^{-9} cm^3 molecule^{-1} s^{-1} (Viggiano et al., 1997) and t is typically 0.05 s under the present experimental setup. $[NO_3^-]$ (that is, $[N^{16}O_3^-]$) was obtained indirectly by measuring its isotope $[N^{18}O_3^-]$ and by taking the natural isotopic ratio of ^{16}O and ^{18}O abundances (99.8%:0.2%) into account. Although $[N^{18}O_3^-]$ varied from day to day, the resulting $[HSO_4^-]/[NO_3^-]$ ratio was fairly constant for a given $[H_2SO_4]$. Before each experimental run, the CIMS was adjusted to obtain $[N^{18}O_3^-]$ between 1500 to 3500 Hz. Thus $[NO_3^-]$ ranged from 8×10^5 to 2×10^6 cm^{-3} and in this condition, 1 Hz of HSO_4^- ion count corresponded to $[H_2SO_4]$ from 1×10^4 to 3×10^4 cm^{-4}. Since the instrument noise of $[HSO_4^-]$ was ~20 Hz, the CIMS detection limit for H_2SO_4 ranged from 2×10^5 to 6×10^5 cm^{-4}. The instrument has performed with a high stability over many hours with the relative standard deviation of <0.1 (Fig. 3a).

3 Numerical simulations of experimental conditions

We have also made several numerical simulations to characterize our experimental conditions in order to provide more constrained $[H_2SO_4]$ and J. We first estimated WLFs by assuming that wall loss is diffusion limited (Sect. 3.1). We then simulated how gas phase species evolve in the nucleation reactor as a function of time (or axial position) of the nucleation reactor (Sect. 3.2). To characterize the nucleation zone, we also simulated J as a function of axial position in the nucleation reactor (Sect. 3.3).

3.1 Wall Loss Factor (WLFs) calculations

WLFs of H_2SO_4 were estimated by assuming that wall loss is a diffusion-limited process based on Hanson and Eisele (2000) (Benson et al., 2008). WLF is defined as:

$$\mathrm{WLF} = \frac{[H_2SO_4]_0}{[H_2SO_4]_t} \quad (8)$$

where $[H_2SO_4]_0$ is the initial concentration, $[H_2SO_4]_t$ is the H_2SO_4 concentration after the time, t, in the nucleation reactor. H_2SO_4 wall loss can be expressed with the first order rate constant, k, in a fast flow reactor:

$$[H_2SO_4]_t = [H_2SO_4]_0\, e^{-kt} \quad (9)$$

k is diffusion-limited (Hanson and Eisele, 2000):

$$k = 3.65\frac{D}{r^2} \quad (10)$$

where D is the diffusion coefficient, and r is the radius of the flow reactor. D=0.094 cm^2 s^{-1} for a RH of 20% and at atmospheric pressure (Hanson and Eisele, 2000). Under the typical experimental conditions (r=2.54 cm), the calculated k is thus 0.053 s^{-1}. In this method, condensation loss is assumed to be negligible. Since wall loss is simply a first order rate process, WLFs can be examined by using different t_r.

Figure 4 shows the calculated WLFs as a function of t_r and RH for different nucleation reactors used in this study (I.D.=5.08 cm and 2.54 cm). At the typical experimental conditions, the estimated WLFs ranged from 1.3 to 12 for t_r from 5–54 s and RH from 11–23% for the nucleation reactor with I.D. 5.08 cm (Fig. 4a). For each figure shown in the present study, we also indicated WLF values, so that the initial $[H_2SO_4]$ conditions can be estimated from the CIMS-measured residual $[H_2SO_4]$ and WLFs.

We have also further verified our calculated WLFs with simultaneous measurements of the initial and the residual $[H_2SO_4]$ with two CIMSs (Fig. 5). These results showed that whether we graph the log J values versus the initial $[H_2SO_4]$ measured at the beginning of the nucleation reactor or versus the residual $[H_2SO_4]$ measured at the end of the nucleation reactor, both plots had similar slopes, indicating that wall loss of H_2SO_4 is indeed a first order process, as assumed in our WLF calculations. Furthermore, the initial concentrations measured were all roughly 2.5 times greater than the residual concentrations under this specific t_r (19 s), which is in a very good agreement with the calculated WLF at the same t_r (Fig. 4a). These results show that WLFs calculated by assuming that wall loss is a diffusion limited process are reasonable.

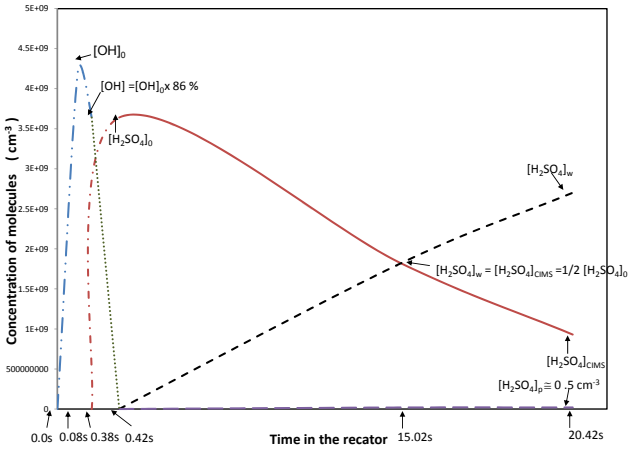

Fig. 6. A simulation of evolution of aerosol precursors in the nucleation reactor for a typical experimental condition, corresponding to those used in Fig. 14 (RH=11%, t_r=19 s, $[SO_2]$=4 ppmv, residual $[H_2SO_4]=1\times10^9$ cm^{-3}). See Sect. 3.2 for the detailed description of this simulation.

3.2 Evolution of aerosol precursors in the nucleation reactor

Figure 6 shows the simulated aerosol precursor concentrations as a function of time in the reactor. The experimental condition shown here corresponds to Fig. 14 (RH=11%, t_r=19 s, $[SO_2]$=4 ppmv, residual $[H_2SO_4]=1\times10^9$ cm^{-3}) (Table 2). $[H_2SO_4]_p$, $[H_2SO_4]_{cims}$, $[H_2SO_4]_w$, and $[H_2SO_4]_0$ indicate the $[H_2SO_4]$ in the particle-phase, that measured by CIMS, that taken on the wall, and the initial concentrations in the nucleation reactor, respectively. $[H_2SO_4]_p$ are calculated based on the volume concentrations from CPC or SMPS measurements, by assuming that the newly formed particles are spherical and are composed of H_2SO_4 and H_2O (with a particle density of 1.4 g cm^{-3}) only. SMPS directly provides volume concentrations. For the CPC data, we derived volume concentrations by assuming that particles are mono-disperse particles with the median diameter of 4 nm. For the data shown in this figure, the particles were measured by the water-CPC. $[H_2SO_4]_0=\mathrm{WLF}\times([H_2SO_4]_{cims}+[H_2SO_4]_p)$. $[H_2SO_4]_w=(\mathrm{WLF}-1)\times([H_2SO_4]_{cims}+[H_2SO_4]_p)$. For most of the experimental conditions, $[H_2SO_4]_{cims} \gg [H_2SO_4]_p$. The gas phase reaction schemes and their rate constants used in this simulation are: (i) H_2O+UV (λ=149.5 nm) $\rightarrow$ OH+H ($J_{H_2O}=9.7\times10^{-6}$ s^{-1} under the typical present

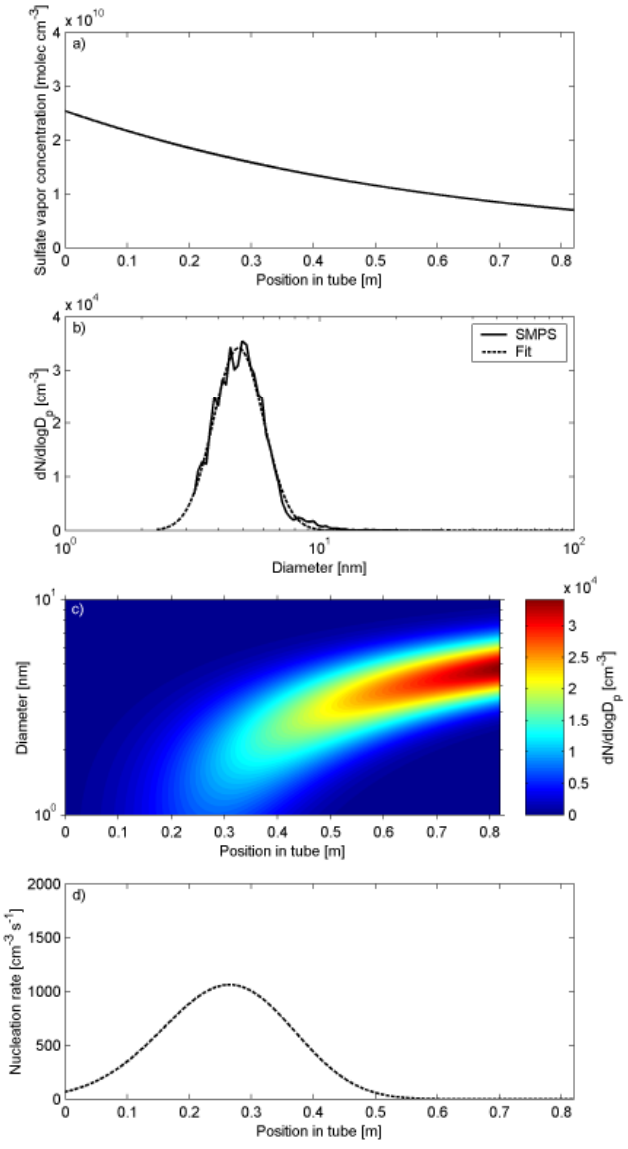

Fig. 7. **(a)** The simulated $[H_2SO_4]$ as a function of axial position in the nucleation reactor, based on the calculated WLFs (Sect. 3.1) and the CIMS-measured residual $[H_2SO_4]$. Experimental conditions used in this figure are the same as those in Fig. 12a with $[SO_2]$ of 4.9 ppmv, except that we used the residual $[H_2SO_4]$ (shown in annotation) of 7×10^9 cm^{-3} (as opposed to 3×10^9 cm^{-3} measured by CIMS) to match the measured D_p and N; the same for Fig. 7c–7d. The H_2SO_4 mass accommodation coefficient was assumed to be unity. **(b)** The measured aerosol size distributions by SMPS along with a fit of this size distribution to a lognormal mode. **(c)** The simulated aerosol size distribution as a function of axial position of the nucleation reactor. **(d)** The simulated J as a function of axial position in the nucleation reactor based on the fitted lognormal size distribution. This simulation results show that nucleation takes place within about 40 cm in the nucleation reactor. This area is considered as the nucleation zone and the t_n=0.5t_r.

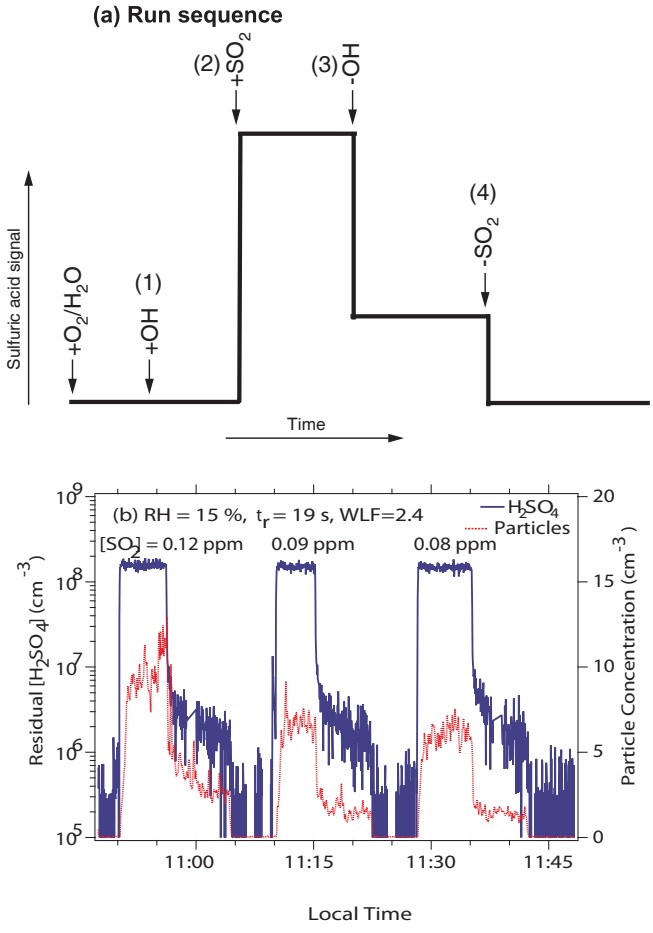

Fig. 8. The experimental procedure and measurement results to investigate the effects of SO_2 and OH on the production of H_2SO_4 and particles at 288 K. **(a)** The experimental run sequence as a function of time. **(b)** The CIMS-measured residual $[H_2SO_4]$ and particle number concentrations in response to running the sequence three times by varying $[SO_2]$. Note the residual $[H_2SO_4]$ is in log scale.

experimental conditions), taking place between 0–0.08 s, (ii) $OH+CO+O_2\rightarrow CO_2+HO_2$ ($k=2.4\times10^{-13}$ cm^3 s^{-1}) (Seinfeld and Pandis, 1997) between 0.08–0.38 s, and (iii) $SO_2+OH\rightarrow HSO_3$ ($k=1.5\times10^{-12}$ cm^3 s^{-1}) (Seinfeld and Pandis, 1997) between 0.38–0.42 s (at $[SO_2]$=4 ppm). Different [OH] will result in different $[H_2SO_4]$. About 86% of the OH radicals generated from water UV photolysis remain after the $CO+OH\ (+O_2)\rightarrow CO_2+HO_2$ reaction for 200 ppbv [CO] impurities (originating from the nitrogen gases blown from liquid nitrogen; experiments with CO scrubbers also confirmed this estimation is reasonable) and a reaction time of 0.38 s (representing the distance of 6 cm from the photolysis region to the point where SO_2 and O_2 are introduced; I.D.=2.54 cm). Thus, the produced initial $[OH]_0=[H_2SO_4]_0/0.86$. Note, the $[OH]_0$ values shown in Fig. 6 are that calculated from this method (that is, 4.4×10^9 cm^{-3}) and is not the [OH] value calculated from

water vapor UV photolysis; however, the derived $[OH]_0$ is in fact the same as the produced [OH] from water UV water photolysis ($[OH]=4\times10^9$ cm^{-3} when t_r=20 s and RH=11%) (Fig. 2b). The nitrogen gages that produce water vapor were introduced at the uppermost region of the flow system and made up the majority of the flow, hence further dilution by SO_2 and O_2 gases is considered not important. As soon as H_2SO_4 is formed, nucleation, condensation and wall loss of H_2SO_4 take place in the nucleation reactor. Because of wall loss, the gas phase $[H_2SO_4]_t=[H_2SO_4]_0e^{-kt}$ (Eq. 9); typically k=0.053 s^{-1} (Sect. 3.1).

3.3 Estimation of the nucleation zone

We developed a simple model of condensational growth in the flow reactor in order to determine where nucleation likely occurs in the reactor. The inputs to the model are the aerosol size distribution and the concentration of H_2SO_4 vapor as a function of the axial position in the reactor. We assume that all particle growth occurs by condensation of H_2SO_4 and water in the kinetic condensation regime (Seinfeld and Pandis, 1997):

$$\frac{dD_p}{dt} = \frac{M_s \overline{c}^a \cdot \alpha \cdot (C_{\text{vap}} - C_{eq})}{2 \cdot \rho} \cdot WR \tag{11}$$

where D_p is the diameter of the particle, t is time, M_s is the molecular weight of H_2SO_4, $\overline{c}^a$ is the mean speed of H_2SO_4 vapor molecules, α is the mass transfer accommodation coefficient, C_{vap} is the concentration of H_2SO_4 vapor, C_{eq} is the equilibrium concentration of H_2SO_4 vapor (taken to be 0), WR is the ratio of the wet diameter (H_2SO_4 and water) to the dry diameter (H_2SO_4 only) and ρ is the density. WR is a function of RH and D_p; however, neglecting the Kelvin effect, it is only a function of RH (e.g., WR=1.4 at RH=23%). To determine the position of nucleation zone in the reactor, we estimate the D_p that particles would have grown to when they exit the reactor as a function of where they nucleated in the reactor (i.e. particles that nucleated early in the reactor will have grown to larger D_p then particles that nucleated late in the reactor). We assume here that particles have a D_p of 1 nm when they nucleate and that effect of coagulation is negligible during the time in the reactor. Knowing the measured size distribution of particles at the exit of the flow reactor we then estimate the J as a function of position in the reactor.

Our simulations show position of the nucleation zone is sensitive to the initial $[H_2SO_4]$ and mass accommodation coefficient of H_2SO_4. Figure 7 shows a typical simulation result using this method. The data used in this simulation correspond to the data shown in Fig. 12a with $[SO_2]$ of 4.9 ppmv (see Table 2 for experimental conditions). All the actual measured experimental conditions were used in this simulation, except for the residual $[H_2SO_4]$, we had to use 7×10^9 cm^{-3} (a little bit higher than the actual 3×10^9 cm^{-3}, but within the uncertainty bounds) to match the measured aerosol sizes while predicting the nucleation zone being entirely within the reactor (Fig. 7b). We also used a high accommodation coefficient (1) for the same reason. The simulated J as function of the axial position of the nucleation reactor shows that the nucleation takes places within about 40 cm region, which is the main conclusion of this simulation. The J showed a peak towards the beginning of the tube, but not at the very beginning as might be expected; however, a lower mass accommodation coefficient or residual $[H_2SO_4]$ would cause this zone to appear earlier in the reactor. Sensitivity studies showed that the length of nucleation zone is not strongly sensitive to these values (not shown), so regardless of these uncertainties, we still can conclude that nucleation takes place across a large region in the nucleation reactor. This estimation is surprisingly similar to the numerical simulations by Wyslouzil (1991b) for methanesalfonic acid and water binary nucleation system (19 s t_n vs. 25 s t_r). However, our estimation results are different from Ball et al. (1999) (4 s t_n vs. 26 s t_r). This difference is probably resulted from the steep temperature gradient in the Ball et al. (1999) set up where hot H_2SO_4 vapor was introduced to a colder nucleation reactor (22°C temperature difference) and under such a condition, one can expect nucleation takes place in a more localized area (or shorter nucleation zone). On the other hand, Wyslouzil (1991a, b) and our experiments were preformed both in relatively constant temperatures between the gas mixer and the nucleation reactor and under this condition, there will be a less localization of nucleation.

Since the nucleation zone (40 cm) was estimated to be a half of the length of the nucleation reactor (80 cm), $t_r \approx 2t_n$. This factor of 2 (t_r vs. t_n) has been taken into account for the J calculations here. When taking into account both this factor of 2 and a factor of 5 ("initial" vs. "steady state" N; Sect. 2.3), the J derived from t_n and the "steady steady" particles are 2.5 times lower than those derived from t_r and the "initial" particles. In the present study, we provide the former, while our previous report by Benson et al. (2008) provided the latter (2 times higher, because of the different length of the nucleation reactor).

4 Observational results

4.1 SO_2, OH, H_2O and O_2 effects on H_2SO_4 and particle production: qualitative test

In order to confirm that nucleation takes place via R1–R3 as designed, we first examined the effects of precursor gases by observing the changes in the production of H_2SO_4 and new particles after adding or removing the gas phase species in question. These are qualitative tests and more detailed results will follow from the next sections. Figure 8 shows how H_2SO_4 and N are affected by SO_2 and OH at RH of 15% and t_r of 19 s. The production of OH was controlled by switching the UV radiation on or off in the presence of H_2O vapor.

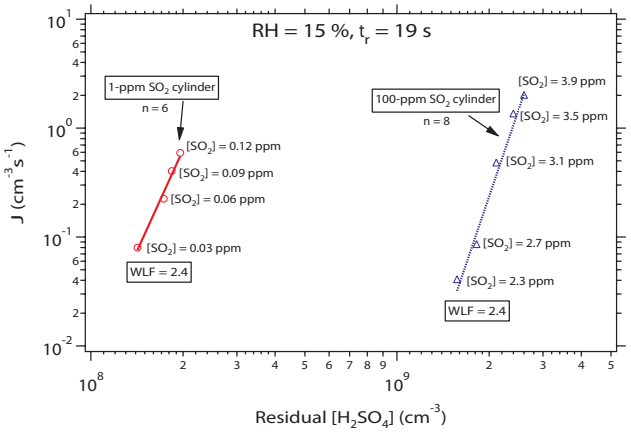

Fig. 9. The measured J as a function of the residual $[H_2SO_4]$ with the 1-ppmv (red circles) and 100-ppmv (blue triangles) SO_2 source cylinders at 288 K. The initial $[SO_2]$ are shown.

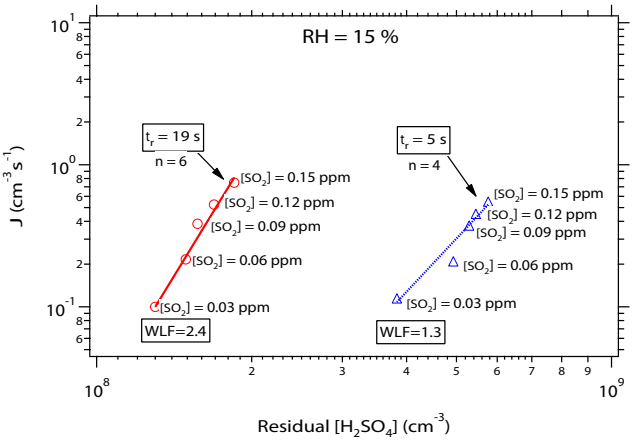

Fig. 10. The measured J as a function of the residual $[H_2SO_4]$ with **(a)** t_r=19 s and **(b)** t_r=5 s at 288 K.

Figure 8a shows the experiment sequence, (1) adding OH, (2) adding OH and SO_2 together, (3) removing OH only, and (4) removing both SO_2 and OH from the flow reactor, in the presence of H_2O vapor and O_2. This sequence was repeated for three runs with different Q_{SO_2} of 0.6, 0.45, to 0.4 lpm. The respective initial SO_2 concentrations $[SO_2]$, calculated based on the SO_2 source concentration and the ratio of the Q_{SO_2} to the Q_{total}, were 0.12, 0.09, and 0.08 ppmv. Figure 8b shows the distinctive rise or drop of $[H_2SO_4]$ when switching the Q_{SO_2} on or off and these results confirm that H_2SO_4 vapor has formed from R1–R3 and new particles formed via nucleation involving H_2SO_4 vapor.

Figure 8b also shows that there was no production of H_2SO_4 and new particles unless SO_2 was added to OH, O_2, and H_2O [steps 1 and 2]. It was consistent throughout our experiments that the background values of $[H_2SO_4]$ and N were negligible in the absence of SO_2, indicating that the experimental setup was well constructed and the flow reactor is fairly clean. However, at step (3) in the absence of OH and in the presence of SO_2, both the $[H_2SO_4]$ and N dropped sharply to a lower level, but above the initial background values (without SO_2). This result was not expected from R1–R3. In addition, since we have used much higher $[SO_2]$ than [OH] (at one order of magnitude higher), $[H_2SO_4]$ should be the same as [OH] and independent of $[SO_2]$ and thus N would also be constant at the same t_n and RH. However, from the first sequence run to the third one, the gradual decrease of $[H_2SO_4]$ from 1.6×10^8 to 1.5×10^8 cm^{-3} and N from 10 to 6 cm^{-3} was a result of the reduced amount of SO_2 added to the system. Figure 9 shows more distinctive dependence of $[H_2SO_4]$ and N on $[SO_2]$ at constant RH and t_r. Similar dependence of N and $[H_2SO_4]$ on $[SO_2]$ can be seen from other figures presented here (Figs. 10–15). This $[H_2SO_4]$ dependence on $[SO_2]$, together with $[H_2SO_4]$ and new particle production in the absence of OH, suggest a possible incomplete mixing between SO_2 and OH and an unknown process of the H_2SO_4 and new particle production, as will be discussed in Sect. 5.5.

With similar experiment sequences, we tested the effects of H_2O on the production of H_2SO_4 and particles. As expected, removing H_2O has reduced the production of both H_2SO_4 and new particles. For example, with the presence of H_2O, $[H_2SO_4]$ and N were 1.6×10^8 cm^{-3} and 9 cm^{-3}, respectively, at RH=15%, whereas with the removal of H_2O, $[H_2SO_4]$ and N were 7.2×10^6 cm^{-3} and 4 cm^{-3}, respectively (not shown). The minimum RH of 4% (as opposed to 0%) was reached by simply not bubbling the water but water was still there; RH sensors also have ±4% accuracy. As will be discussed in Sect. 4.4, there were RH effects on both the measured N and D_p.

In contrast to the cases of SO_2, OH and water, the removal of O_2 from the system had only minor effects on the production of H_2SO_4 and new particles. With or without O_2, the $[H_2SO_4]$ and N were nearly the same. In addition, both the $[H_2SO_4]$ and N became more fluctuating without O_2. The lack of O_2 effects was not expected because SO_3 would not form without O_2, according to R2. We believe there was no leak into the system from the room air, because the pressure of the flow reactor was always maintained above the ambient pressure. Some O_2 may have come from the gas cylinders as a part of the impurities. But since O_2 effects are not the focus of the present study, we did not attempt to investigate the source of O_2 impurities or detect its concentrations.

Lower concentrations of SO_2 were used by diluting standard SO_2 gases (1 and 100 ppmv), to obtain a given J value. We also have seen that a substantially higher initial $[SO_2]$ was required when diluting the SO_2 from the 100 ppmv cylinder than from the 1 ppmv cylinder (Fig. 9). Figure 9 shows the measured $[H_2SO_4]$ and N at RH of 15%, Q_{total} of 5 lpm and t_r of 19 s. For example, an initial $[SO_2]$ of 3 ppmv was required for the 100-ppmv experiment to obtain J of 0.5 cm^{-3} s^{-1}, while only 0.1 ppmv SO_2 was required for the

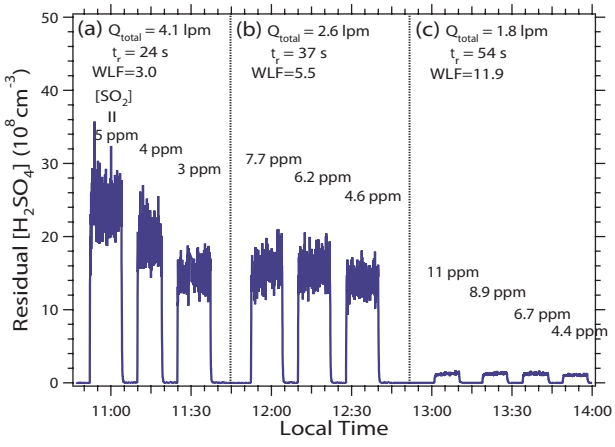

Fig. 11. The CIMS-measured residual $[H_2SO_4]$ at varying total flow rate Q_{total} and t_r at RH of 23% and 288 K. The measured number size distributions of these particles are shown in Fig. 12.

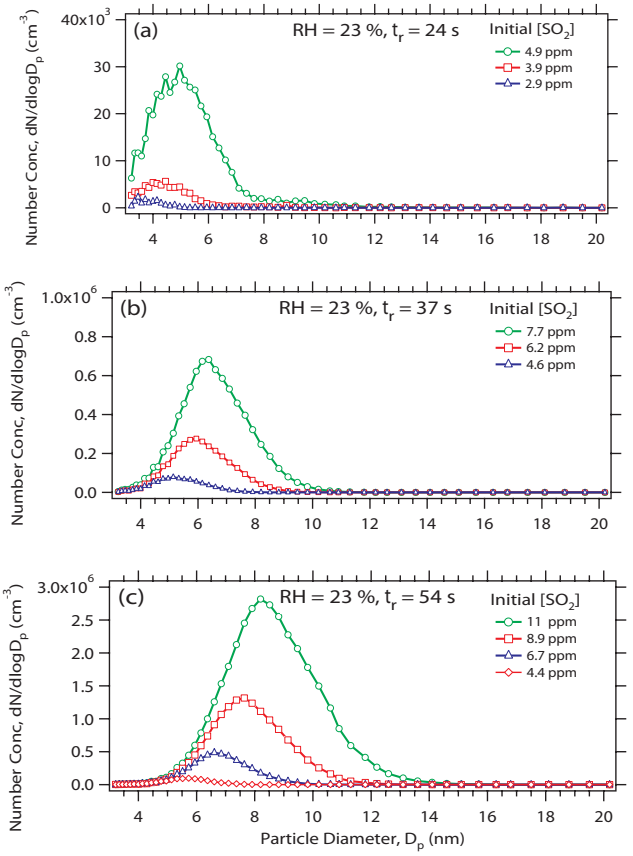

Fig. 12. The average number size distributions of newly formed particles at varying total flow rates Q_{total}, initial SO_2 concentrations, and t_r of **(a)** 24 s, **(b)** 37 s, and **(c)** 54 s. These datasets are the same as those used in Fig. 11. Note the scales of the y-axes are different.

1-ppmv experiment to form similar numbers of new particles. This difference occurs probably because of the incomplete mixing of SO_2 gases with other gas species in the fast flow reactor. Because SO_2 molecules were released near the centerline of the flow reactor, it would take a longer time for SO_2 molecules to be vigorously mixed with OH radicals at lower mixing ratios than at higher mixing ratios. The flow ratios of Q_{SO_2} to Q_{total} were from 0.03–0.15 and from 0.025–0.04 for the 1 ppmv- and 100 ppmv-SO_2 cylinder experiments, respectively. Because its Q_{SO_2} to Q_{total} ratios were larger than that for the 100-ppmv cylinder experiment, we can expect a better mixing with the 1-ppmv cylinder.

4.2 Residence time (t_r) dependence of particle numbers (***N***) and residual $[H_2SO_4]$

We have observed that t_r affects the measured particle number concentrations and the residual $[H_2SO_4]$ (Fig. 10). t_r was varied between 5 and 19 s, by using two nucleation tubes with similar lengths (L of 80 cm and 82 cm) but different diameters (ID=2.54 cm and 5.08 cm) at Q_{total} of 5 lpm and RH of 15%. The initial $[SO_2]$ varied from 0.03 to 0.15 ppmv in the two experiments and were identical for these two different t_r at the constant Q_{total}. The calculated J from the experiments with t_r of 5 s and 19 s were on the same order of magnitude (0.1–0.54 $cm^{-3}\,s^{-1}$ vs. 0.1–0.75 $cm^{-3}\,s^{-1}$), but the CIMS-measured $[H_2SO_4]$ were different. In fact, the $[H_2SO_4]$ at t_r of 5 s was about a factor of two higher than that at t_r of 19 s (3.8×10^8 to 5.8×10^8 cm^{-3} vs. 1.3×10^8 to 1.9×10^8 cm^{-3}). Since the J values were comparable, it is likely that the $[H_2SO_4]$ difference was caused by the increased wall loss at longer t_r (Fig. 4a; Sect. 3.1).

4.3 Number concentrations (N) vs. particle sizes (D_p)

We also investigated how N and D_p vary as a function of t_r and the initial $[SO_2]$ at constant RH (e.g., 23%) (Figs. 11–13). In this series of experiments, Q_{total} was decreased to increase t_r and the initial $[SO_2]$. At RH of 23% and t_r of 24 s, when the initial $[SO_2]$ was raised from 2.9 to 4.9 ppmv, N increased from 220 to 6.9×10^3 cm^{-3} and D_p increased from 3.6 to 5.0 nm (Fig. 12a). The corresponding $[H_2SO_4]$ ranged from 1.5×10^9 to 2.4×10^9 cm^{-3} (Fig. 11). Such increases of N and D_p with increasing initial $[SO_2]$ were even more substantial at the t_r of 54 s; the N increased from 1.4×10^4 to 5.5×10^5 cm^{-3} and the D_p increased from 5.6–8.2 nm when the initial $[SO_2]$ increased from 4.4–11.1 ppmv (Fig. 12c). As t_r increased from 24–54 s, with similar initial $[SO_2]$ (4.9, 4.6, and 4.4 ppmv), N also increased from 6.9×10^3 to 1.4×10^4 cm^{-3} and the D_p increased from 5.0–5.7 nm (Fig. 13). These results show that both $N$and D_p increase with increasing t_r; N becomes higher because of nucleation and D_p larger because of condensation growth. But since both D_p and $N$are affected by t_r, this makes estimation

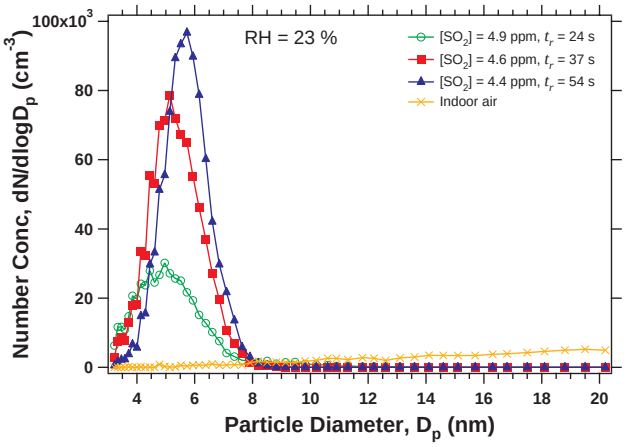

Fig. 13. The average number size distributions measured at similar initial $[SO_2]$ but varying t_r of 24 s (green circles), 37 s (red squares), and 54 s (blue triangles) at 288 K. These datasets are also shown in Figs. 11 and 12. In comparison, an average aerosol size distribution measured from room air is also shown (orange crosses).

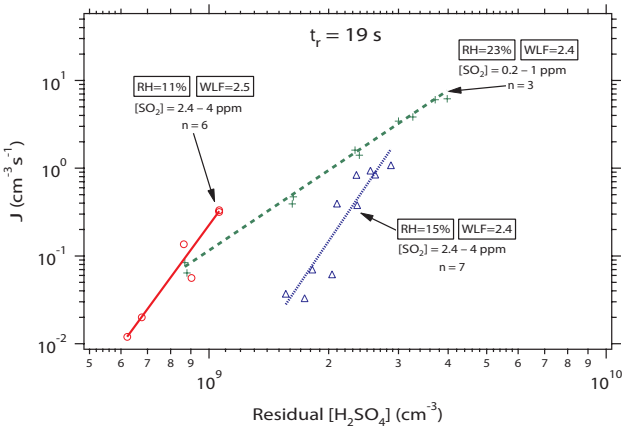

Fig. 14. The measured J as a function of the residual $[H_2SO_4]$ at **(a)** RH=11%, **(b)** RH=15%, and **(c)** RH=23% at 288 K.

of "apparent" J from different nucleation studies less comparable, especially when particles have different D_p under different t_r (or t_n) conditions.

4.4 The RH effects on nucleation rate (J) and particle size (D_p)

Figure 14 shows the RH effects on the production of H_2SO_4 and particles at constant t_r (e.g., 19 s). Q_{total} (5 lpm) and the nucleation reactor's ID (5.08 cm) and L (82 cm) were identical for these three RH levels. The initial $[SO_2]$ was between 2.4–4 ppmv for RH of 11–15%, while the initial $[SO_2]$ was between 0.2–1 ppmv for RH of 23%. At $[SO_2]$ of 2.4 ppmv, for example, when the RH was raised from 11–15%, the $[H_2SO_4]$ and J nearly tripled from 6.2×10^8 to 1.7×10^9 cm^{-3} and 0.01 to 0.03 cm^{-3} s^{-1}, respectively. This shows higher productions of H_2SO_4 and N at higher RH.

Figure 15 shows the particle size distributions measured at Q_{SO_2} of 0.1 lpm, Q_{total} of 2.6 lpm, the initial $[SO_2]$ of 3.8 ppmv, and t_r of 38 s for RH of 22%, 26%, and 30%. As RH increased from 22 to 30%, the CIMS-measured $[H_2SO_4]$ increased from 7.3×10^8 to 1.0×10^9 cm^{-3} and N increased from 5.9×10^3 to 1.1×10^5 cm^{-3}. The mode diameter also increased from 5.1–6.4 nm with increasing RH due to the increased H_2SO_4 production and particle growth.

5 Discussions

5.1 Technical factors that affect nucleation rate (J) calculations

Several competing processes simultaneously take place in the nucleation reactor, such as nucleation, wall loss, and coagulation and condensation growth (Fig. 16). These processes also affect the measured residual $[H_2SO_4]$, N, and D_p, and in turn, affect the calculated J and the J dependence on $[H_2SO_4]$ (Fig. 17).

We have seen lower residual $[H_2SO_4]$ at longer t_r (Figs. 10 and 11), consistent with that wall loss of H_2SO_4 is a first order loss rate process (Sect. 3). Wall loss can be a limitation of flow tube experiments, especially for nucleation reactors that have large surface to volume ratios (e.g., with small inner diameters). In addition to wall loss, some other factors (e.g., RH) can affect the residual $[H_2SO_4]$ and N. In the present experimental setup, H_2O molecules participate in both the H_2SO_4 formation and aerosol nucleation process. This is because increasing $[H_2O]$ would increase the [OH] and thus H_2SO_4 production (R1), and also favor hydration of H_2SO_4 molecules. High RH can also increase penetration efficiency of H_2SO_4. The addition of H_2O molecules to H_2SO_4 molecules can also reduce diffusion coefficients and thus decrease wall loss, although the RH effects on WLFs are less important than the t_r effects (Fig. 4).

Our results also show that both the N and D_p vary as a function of $[H_2SO_4]$, RH and t_n (Figs. 12, 13, 15). Also, at high t_r, the condensation growth and wall loss of H_2SO_4 will become more important. At higher J values, N can be even anti-correlated with $[H_2SO_4]$ (Benson et al., 2008), because condensation growth can dominate over nucleation processes with larger particle surface areas (at higher N and D_p). If the time scale of coagulation process is comparable to that of the nucleation process, it will lead to the reduced N and subsequently underestimated J (Wyslouzil et al., 1991a). Under such a circumstance, the underestimated J at the high end of the concentration range will in turn reduce the steepness of the slope of the power relationship between J and $[H_2SO_4]$. To obtain accurate "apparent" J, nucleation experiments must be conducted below the level at which nucleation dominates over coagulation or condensation growth

process, for example, at lower $[H_2SO_4]$, lower N and shorter t_r. To reduce such effects of condensation and coagulation on the measured J values, the measured N can be extrapolated at a specific D_p (e.g., 1 nm) (Kerminen and Kulmala, 2002; Kulmala et al., 2006). This normalization would allow one to obtain J values that are more representative of the "true" J (i.e., the formation rate of the critical clusters) under different experimental conditions. In the present study, however, we report the measured "apparent" J to directly compare with other laboratory experiments.

5.2 Dependence of nucleation rates (J) on $[H_2SO_4]$, RH and residence time (t_r)

A summary of the measured $[H_2SO_4]$ and J at 288 K, 97.3 kPa, and RH of 11%, 15%, and 23% is given in Table 2. The residual $[H_2SO_4]$ (measured by CIMS at the end of the nucleation reactor) ranged from 9×10^7 to 1×10^{10} cm^{-3} and the initial $[H_2SO_4]$ (calculated from the residual $[H_2SO_4]$ and WLFs) ranged from 2×10^8 to 2×10^{10} cm^{-3}. Under our experimental conditions, the measured J ranged from 0.01–220 cm^{-3} s^{-1}. Figure 17 shows the plots of log J vs. log $[H_2SO_4]$ for the entire data taken from our nucleation study (Table 2). We also included here the J values cited from earlier studies by Ball et al. (1999) and Berndt et al. (2006) for comparison. The data points from the present study fall between those from these two earlier studies. In order to measure the H_2SO_4/H_2O binary J of 1 cm^{-3} s^{-1}, the minimum residual $[H_2SO_4]$ (as well as the initial $[H_2SO_4]$) was in the 10^8–10^9 cm^{-3} range at RH between 11–23% and 288 K (Fig. 17a). In Berndt et al. (2005, 2006), however, the residual $[H_2SO_4]$ of 10^6–10^7 cm^{-3} was sufficient to produce J of 1 cm^{-3} s^{-1} at RH of 11%, 22%, and 288 K. In Ball et al. (1999), $[H_2SO_4]$ of $\sim10^9$ cm^{-3} was needed at RH between 2–15% and 295 K for binary and ternary (with NH_3) homogeneous nucleation. In comparison, predictions from classical nucleation theory showed that the initial $[H_2SO_4]$ has to be at least 10^{10} cm^{-3} to observe significant binary J at RH<20% and 298 K (Vehkamäki et al., 2002). A recent kinetic quasi-unary nucleation model for H_2SO_4/H_2O also showed that the initial $[H_2SO_4]$ has to be at least 10^{11} cm^{-3} to observe significant binary J at RH<20% and 300 K (Yu, 2006).

We estimated $n_{H_2SO_4}$ from 3–8 under our experimental conditions (Fig. 17). The slopes of log J vs. log $[H_2SO_4]$ at RH of 23% were not as steep as that at RH of 11% and 15%; $n_{H_2SO_4}$ increased from ~3 to ~8 when RH decreased from 23% to 15% (Fig. 17a). These results indicate that there are less $n_{H_2SO_4}$ at higher RH, as predicted from the nucleation theories. The increased $n_{H_2SO_4}$ with decreasing RH is consistent with nucleation theories and also consistent with Ball et al. (1999) and Berndt et al. (2005, 2006) results (Fig. 17b). The $n_{H_2SO_4}$ at RH of 15%, however, is not distinctly different from that at RH of 11% (4–8 vs. 3–6). Interestingly, the n_{H2SO4} values at RH of 15% and 10% from Ball et al. (1999) were also not very different from each other (7 vs. 8). Nevertheless, the $n_{H_2SO_4}$ value increased from 7 to 13 when the RH was lowered from 15 to 2% in Ball et al. (1999). The data points from this study (group B) at RH of 15% and t_n of 19 s (from 100 ppmv source cylinder experiments) nearly overlap with those from Ball et al. (1999)'s liquid H_2SO_4 experiments at RH of 15%. The $n_{H_2SO_4}$ obtained from laboratory studies of H_2SO_4/H_2O binary homogenous nucleation is typically larger than 3 and even up to ~30 for $[H_2SO_4]$ between ~10^7 to 10^{11} molecules cm^{-3} (this study; Wyslouzil et al., 1991; Viisanen et al., 1997; Ball et al., 1999; Berndt et al., 2005, 2006; Benson et al., 2008). These numbers are much higher than those actually observed in the atmospheres. Field studies have shown that that $n_{H_2SO_4}$ is often between 1–2 (Weber et al., 1996; Sihto et al., 2006; McMurry and Eisele, 2005). Such a discrepancy raises questions on whether the binary homogeneous nucleation is the primary nucleation mechanism in the atmosphere. Recently, Kulmala et al. (2006) proposed an activation theory of neutral clusters containing one or two H_2SO_4 molecules to explain the field observations. While field studies of small neutral clusters (Kulmala et al., 2007a) also support this theory, further experimental work will be required to prove this new theory.

Recent findings by Winkler et al. (2008) showed that organic vapors can easily condense on small charged, preexisting seed aerosol particles starting from 1.2 nm and undergo heterogeneous nucleation at lower saturation ratios. Since we have not intentionally applied any ion sources in the nucleation reactor, with the low production rates of ions being only the natural sources at the ground level (Lovejoy et al., 2004) there are minimal charged clusters or small particles that can act as seed particles for heterogeneous nucleation. We also believe that there are minimum organic vapor concentrations in our system and therefore, heterogeneous nucleation on charged clusters is negligible. But this is an interesting area we want to look into in the future.

5.3 Particle growth rates

Based on these measured D_p, we calculated aerosol growth rates using three different methods. In the first method, growth rates were calculated based on the measured aerosol size distributions as a function of t_r. The aerosol geometric mean diameters (GMDs) were 5.1 to 5.3, to 5.7 nm for t_r of 24 to 37, to 54 s, respectively (Table 3), for the size distributions shown in Fig. 13, for example. Growth rates derived from this first method were 95 nm h^{-1}. The second method uses the same GMDs and t_r, but we assume that these particles have grown from critical cluster size 1.5 nm (Kumala et al., 2007a) to the measured GMDs within these t_r. The growth rates calculated from this second method ranged from 200–500 nm h^{-1}. The third method is a kinetic method based on the initial $[H_2SO_4]$ (calculated from the residual $[H_2SO_4]$ and WLFs) and mass accommodation coefficient (1). This method provides growth rates similar to those derived from

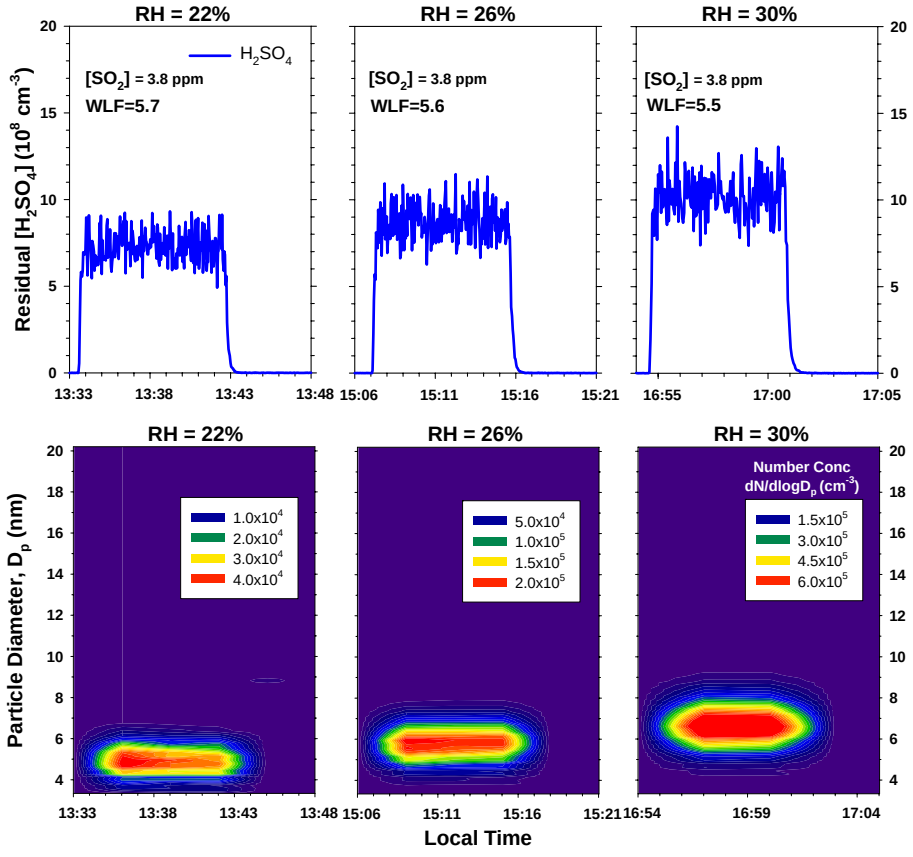

Fig. 15. The CIMS-measured residual H_2SO_4 and number size distributions of newly formed particles at **(a)** RH=22% (left panels), **(b)** RH=26% (middle panels), and **(c)** RH=30% (right panels) at 288 K. Note the scales for the number concentration are different (lower panels).

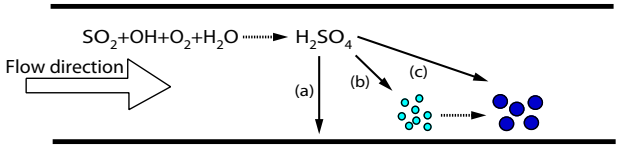

Fig. 16. Hypothetical loss processes for gas phase H_2SO_4 molecules that take place during the formation of H_2SO_4 from the SO_2+OH→HSO_3 reaction in the flow reactor and the subsequent particle nucleation. Solid arrows indicate three pathways related to gas phase H_2SO_4 losses, **(a)** wall loss, **(b)** nucleation, and **(c)** condensation on the formed particles. Also see Fig. 6 for the simulation of $[H_2SO_4]$ vs. time in the nucleation reactor.

the second method. The concept used in the third method is very similar to that used in our independent simulations of nucleation zone (Sect. 3.3) and in fact, similar growth rates were also derived from the nucleation zone simulations. These calculated growth rates were all much higher than those observed in the atmosphere, due to the fact that the particle precursor concentrations used in our nucleation experiments (10^8–10^9 cm^{-3}) were much higher than the typical atmospheric conditions (10^6–10^7 cm^{-3}). The derived growth rates from field studies usually range from 1–20 nm h^{-1} (Kulmala et al., 2004), although there are a few exceptions from recent reports. Svenningsson et al. (2008) have shown particle growth rates up to 50 nm h^{-1} in a rural background station in northern Sweden. Iida et al. (2008) also showed growth rates ranging from 15–40 nm h^{-1} in Tacamec, Mexico, much higher than those reported from other urban areas.

5.4 Formation of H_2SO_4 and particles in the absence of OH and UV

Although it is not the focus of the present study, it is worthwhile to mention that we also observed that H_2SO_4 and particle formation in the absence of OH, i.e., only from SO_2, O_2, and water vapor. There are several experimental results related to this feature. First, as shown in Fig. 8, there were some measurable amounts of H_2SO_4 and particles when UV was off (the residual $[H_2SO_4]$ measured without OH and UV

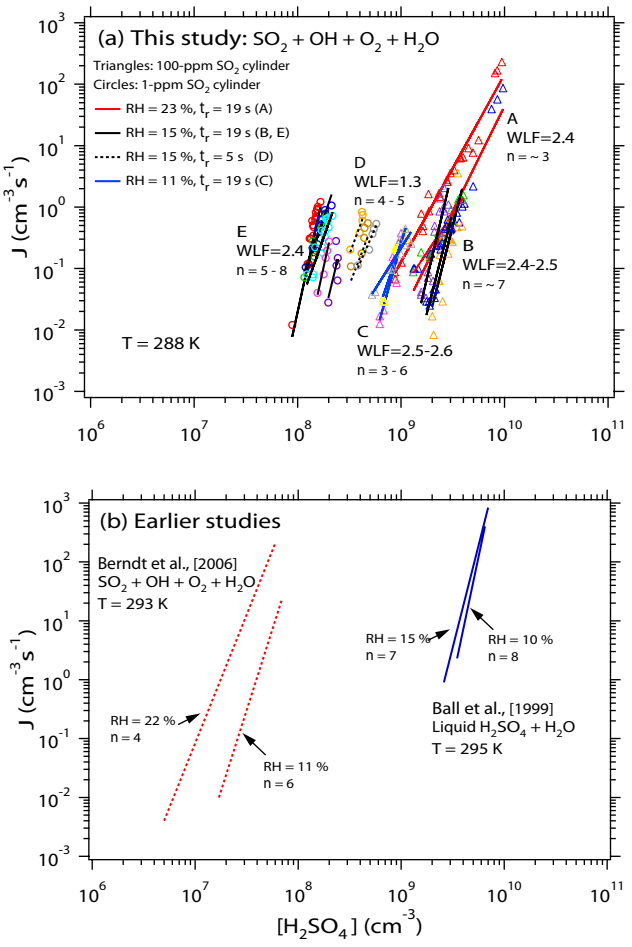

Fig. 17. The measured J as a function of the residual $[H_2SO_4]$ for **(a)** the present SO_2+OH experiments and **(b)** from earlier studies. The linear lines are the results of power regression on the experimental data. The calculated WLFs corresponding to our experimental conditions are shown so that the initial $[H_2SO_4]$ can be estimated. See Table 2 for the detailed experimental conditions. In Ball et al. (1999) where liquid H_2SO_4 sample was used, WLF=22. Berndt et al. (2006) where the SO_2+OH reaction was used have not provided WLFs.

were usually at least one or two orders of magnitude lower than those produced in the presence of UV and OH); we also saw the same feature when starting with SO_2 but UV off. Such a feature consistently appeared over different time periods and even after we washed the flow tube with distilled water overnight to remove all H_2SO_4 and particles deposited on it from previous experiments. In addition, the measured $[H_2SO_4]$ and particles were also directly related to the initial $[SO_2]$ (Figs. 9–15), even though $[SO_2] \gg [OH]$ and therefore, the produced $[H_2SO_4]$ from R1 should be the same as [OH] and independent from $[SO_2]$. These results may suggest that there are some other pathways for H_2SO_4 and particle formation, independent from R1–R3. But we do not understand the reaction and nucleation mechanisms from these

Table 3. Lognormal distribution parameters of the measured aerosol sizes (corresponding to Fig. 13) used for aerosol growth rate calculations (Sect. 5.3). GMD indicates geometric mean diameter.

Residence Time, t_r (s)	GMD (nm)	Width (nm)	Particle Conc. (cm^{-3})
24	5.1	1.25	8136
37	5.3	1.18	14 232
54	5.7	1.14	14 941

qualitative results at present and it is also difficult to know if these results have something to do with Berndt et al. (2008) and Stratmann et al. (2008)'s speculation of an alternative path for new particle formation involving HSO_5.

6 Conclusions

We have developed a laboratory experimental set up to study the binary homogeneous nucleation H_2SO_4/H_2O. This setup design is largely based on Ball et al. (1999), Zhang et al. (2004) and Berndt et al. (2005, 2006). Specifically, our nucleation reactor has similar dimensions and flow rates as in Ball et al. (1999) and both these two studies directly measure $[H_2SO_4]$ with CIMS at the end of the nucleation reactor. We also produce H_2SO_4 vapor in-situ from the SO_2+OH→HSO_3 reaction similarly to Berndt et al. (2005, 2006). However, unlike Berndt et al. (2005, 2006) where OH is produced from ozone photolysis and its concentrations are calculated from titration reactions with CO and hydrocarbon compounds, in our study OH is produced from water UV absorption, which also allows for direct measurements of [OH], with accurate photon flux measurements, and thus the initial $[H_2SO_4]$. While Ball et al. (1999) have used a movable tube to sample particles to determine the nucleation zone, we used a numerical simulation to characterize the nucleation zone based on the measured $[H_2SO_4]$ and D_p. WLFs were determined from calculations by assuming that wall loss is diffusion limited based on Hanson and Eisele (2000) and also from simultaneous measurements of the initial and residual $[H_2SO_4]$ with two CIMSs and these results are consistent each other. These WLFs allow us to provide both the initial and residual $[H_2SO_4]$ from the CIMS-measured residual $[H_2SO_4]$. In the present study, we provide a systematic evaluation of this new nucleation experimental system from various technical aspects and discuss our primarily BHN results by comparing with other laboratory studies.

The H_2SO_4/H_2O BHN J values were measured using SO_2+OH→HSO_3 at 288 K, 97.3 kPa, RH from 11–23% for the H_2SO_4 residual concentrations from 10^8–10^{10} cm^{-3} and t_r between 5–54 s. In our system, the nucleation zone is about half of the nucleation reactor and thus t_n=0.5t_r. The measured J ranged from 0.01–220 $cm^{-3}\,s^{-1}$ and increased

with increasing $[H_2SO_4]$ and RH. Such trends are consistent with the predictions of nucleation theories. Under our experimental conditions, $[H_2SO_4]$ of 10^8–10^9 cm^{-3} (both initial and residual concentrations) was needed to produce the J of 1 cm^{-3} s^{-1}. This $[H_2SO_4]$ threshold is much higher than the atmospheric conditions (10^6–10^7 cm^{-3}) but falls between those in Berndt et al. (2005, 2006) (10^6–10^7 cm^{-3}) and in Ball et al. (1999) (10^9–10^{10} cm^{-3}). The power relationship between measured J and $[H_2SO_4]$ suggests $n_{H_2SO_4}$ ranged from 3–8 H_2SO_4. This number also increased with decreasing RH, in an agreement with classical nucleation theories, and is in the same range as those reported from the previous laboratory nucleation studies (Wyslouzil et al., 1991b; Ball et al., 1999; Berndt et al., 2005, 2006). These estimated $n_{H_2SO_4}$ from these laboratory studies are, however, much larger than those derived from field observations (1–2) (Weber et al., 1996; Sihto et al., 2006; McMurry and Eisele, 2005). These different $n_{H_2SO_4}$ derived from the laboratory studies and atmospheric observations, together with the higher threshold of $[H_2SO_4]$ required for nucleation in the laboratory studies than the atmospheric conditions, indicate that other ternary species are important for atmospheric aerosol nucleation and growth. The measured sizes of newly-formed particles were smaller than 10 nm. The derived growth rates calculated from the measured $[H_2SO_4]$, D_p and t_r ranged from 100–500 nm h^{-1}, much higher than atmospheric observations, because of high $[H_2SO_4]$ used in our study.

At present there are large discrepancies between different nucleation experiments and it is important to understand what factors cause such differences. There are several important technical issues we have to address, including wall loss, ratios of t_n vs. t_r (or characterization of nucleation zone), nucleation reactor's dimensions, the method to produce H_2SO_4 and detect them, characterization of aerosol sizes in addition to aerosol number concentrations, stability of experimental conditions, and the effects of ternary species. Wall loss is a function of t_r, nucleation tube diameter, and RH. t_n may be different from t_r depending on where the nucleation zone is and the differences depend on the experimental setup and aerosol precursor concentrations. Also, particle measurements often require a long time (e.g., 3 h in the present study) for the system to be stabilized and thus in order to provide reproducible data, the system has to achieve this steady state under each experimental condition, although this can be a time-consuming and somewhat impractical process. Also, many experimental parameters affect each other. For example, not only did aerosol numbers vary but also the sizes vary with aerosol precursor concentrations and t_n (and t_r), so it is necessary to know aerosol sizes to correctly characterize J. In addition, condensation loss of $[H_2SO_4]$ can become significant at high $[H_2SO_4]$ and RH, longer t_r and larger D_p. These complex "matrix" effects should be taken into account, in order to make a valid comparison of J and $[H_2SO_4]$ needed for nucleation from different nucleation studies.

Our future goal is to measure J at atmospherically relevant conditions with $[H_2SO_4]$ in the 10^6–10^7 cm^{-3} range with and without ternary species and compare them with atmospherically observed J. Thus far, our experiments shown here were made at higher $[H_2SO_4]$ ranging from 10^8–10^{10} cm^{-3}. Despite the various technical challenges and difficulties, our nucleation experiments complement other nucleation laboratory studies and provide important kinetics properties of H_2SO_4/H_2O binary homogeneous nucleation and the relatively constrained aerosol precursor concentrations, which are required to test nucleation theories.

Acknowledgements. This study was supported by the NSF CAREER Award (ATM-0645567). We thank Greg Huey and Dave Tanner for the CIMS construction and technical support, Chris Cantrell and Dave Tanner for providing information on designing the OH water vapor UV absorption cell, Jim Gleeson for the help on OH measurements, and Barbara Wyslouzil, Peter Adams, Neil Donahue, Fred Eisele, Kari Lehitnen, and Peter McMurry for useful discussions.

Edited by: A. Laaksonen

References

Ball, S. M., Hanson, D. R., Eisele, F. L., and McMurry, P. H.: Laboratory studies of particle nucleation: Initial results for H_2SO_4, H_2O, and NH_3 vapors, J. Geophys. Res., 104, 23 709–23 718, 1999.

Baron, P.A. and Willeke, K.: Aerosol Measurement: Principles, Techniques, and Applications, 2nd ed., John Wiley and Sons, New York, 2001.

Benson, D. R., Young, L. H., Kameel, F. R., and Lee, S.-H.: Laboratory-measured nucleation rates of sulfuric acid and water binary homogeneous nucleation from the SO_2 + OH reaction, Geophys. Res. Lett., 35, L11801, doi:10.1029/2008GL033387, 2008.

Berndt, T., Böge, O., Stratmann, F., Heintzenberg, J., and Kulmala, M.: Rapid formation of sulphuric acid particles at near-atmospheric conditions, Science, 307, 698–700, 2005.

Berndt, T., Böge, O., and Stratmann, F.: Formation of atmospheric H_2SO_4/H_2O particles in the absence of organics: a laboratory study, Geophys. Res. Lett., 33, L15817, doi:10.1029/2006GL026660, 2006.

Berndt, T., Stratmann, F., Bräsel, S., Heintzenberg, J., Laaksonen, A., and Kulmala, M.: SO_2 oxidation products other than H_2SO_4 as a trigger of new particle formation – Part 1: Laboratory investigations, Atmos. Chem. Phys. Discuss., 8, 9761–9782, 2008, http://www.atmos-chem-phys-discuss.net/8/9761/2008/.

Boulaud, D., Madelaine, G., Vigla, D., and Bricard, J.: Experimental study on the nucleation of water vapor sulphuric acid binary system, J. Chem. Phys., 66, 4854–4860, 1977.

Cantrell, C. A., Zimmer, A., and Tyndall, G. S.: Absorption cross sections for water vapor from 183 to 193 nm, Geophys. Res. Lett., 24, 2195–2198, 1997.

Christensen, P. S., Wedel, S., and Livbjerg, H.: The kinetics of the photolytic production of particles from SO_2 and NH_3 in humid air, Chem. Eng. Sci., 49, 4605–4614, 1994.

DeMore, W. B., Sander, S. P., Golden, D. M., Hampson, R. F., Kurylo, M. J., Howard, C. J., Ravishankara, A. R., Kolb, C. E., and Molina, M. J.: Chemical Kinetics and Photochemical Data for Use in Stratospheric Modeling, Evaluation number 12, JPL Publ. 97-4, NASA Jet Porpulsion Lab., Pasadena, Calif., 1997.

Diamond, G. L., Iribarne, J. V., and Corr, D. J.: Ion-induced nucleation from sulphur dioxide, J. Aerosol Sci., 16, 43–55, 1985.

Eisele, F. L. and Tanner, D. J.: Measurement of the gas-phase concentration of H_2SO_4 and methane sulphonic-acid and estimates of H_2SO_4 production and loss in the atmosphere, J. Geophys. Res., 98, 9001–9010, 1993.

Hanson, D. R. and Eisele, F.: Diffusion of H_2SO_4 in humidified nitrogen: Hydrated H_2SO_4, J. Phys. Chem. A, 104, 1715–1719, 2000.

Heist, R. H. and He, H.: Review of vapor to liquid homogeneous nucleation experiments from 1968 to 1992, J. Phys. Chem. Ref. Data, 23, 781–805, 1994.

Huey, L. G.: Measurement of trace atmospheric species by chemical ionization mass spectrometry: Speciation of reactive nitrogen and future directions, Mass Spectrom. Rev., 26, 166–184, 2007.

Iida, K., Stolzenburg, M. R., McMurry, P. H., and Smith, J. N.: Estimating nanoparticle growth rates from size-dependent charged fractions: Analysis of new particle formation events in Mexico City, J. Geophys. Res., 113, D05207, doi:10.1029/2007JD009260, 2008.

Kashchiev, D.: On the relation between nucleation work, nucleus size and nucleation rate, J. Chem. Phys., 76, 5098–5102, 1982.

Kerminen, V.-M. and Kulmala, M.: Analytical formulae connecting the "real" and the "apparent" nucleation rate and the nuclei number concentration for atmospheric nucleation events, J. Aerosol Sci., 33, 609–622, 2002.

Kim, T. O., Adachi, M., Okuyama, K., and Seinfeld, J. H.: Experimental measurement of competitive ion-induced and binary homogeneous nucleation in $SO_2/H_2O/N_2$ mixtures, Aerosol Sci. Technol., 26, 527–543, 1997.

Korhonen, P., Kulmala, M., Laaksonen, A., Viisanen, Y., McGraw, R., and Seinfeld, J. H.: Ternary nucleation of H_2SO_4, NH_3, and H_2O in the atmosphere, J. Geophys. Res., 104, 26 349–26 353, 1999.

Kulmala, M., Vehkamäki, H., Petäjä, T., Dal Maso, M., Lauri, A., Kerminen, V.-M., Birmili, W., and McMurry, P. H.: Formation and growth rates of ultrafine atmospheric particles: a review of observations, J. Aerosol. Sci., 35, 143–176, 2004.

Kulmala, M., Lehtinen, K. E. J., and Laaksonen, A.: Cluster activation theory as an explanation of the linear dependence between formation rate of 3 nm particles and sulphuric acid concentration, Atmos. Chem. Phys., 6, 787–793, 2006, http://www.atmos-chem-phys.net/6/787/2006/.

Kulmala, M., Riipinen, I., Sipilä, M., Manninen, H. E., Petäjä, T., Junninen, H., Dal Maso, M., Mordas, G., Mirme, A., Vana, M., Hirsikko, A., Laakso, L., Harrison, R. M., Hanson, I., Leung, C., Lehtinen, K. E. J., and Kerminen, V.-M.: Toward direct measurement of atmospheric nucleation, Science 318, 89–92, doi:10.1126/science.1144124, 2007a.

Kulmala, M., Mordas, G., Petäjä, T., Grönholm, T., Aalto, P. P., Vehkamäki, H., Hienola, A. I., Herrmann, E., Sipilä, M., Riipinen, I., Manninen, H., Hämeri, K., Stratmann, F., Bilde, M., Winkler, P. M., Birmili, W., and Wagner, P. E.: The condensation particle counter battery (CPCB): A new tool to investigate the activation properties of nanoparticles, J. Aerosol Sci., 38, 289–304, 2007b.

Laaksonen, A., Talanquer, V., and Oxtoby, D. W.: Nucleation: measurements, theory, and atmospheric applications, Annu. Rev. Phys. Chem., 46, 489–524, 1995.

Laaksonen, A., Kulmala, M., Berndt, T., Stratmann, F., Mikkonen, S., Ruuskanen, A., Lehtinen, K. E. J., Dal Maso, M., Aalto, P., Petj, T., Riipinen, I., Sihto, S.-L., Janson, R., Arnold, F., Hanke, M., Ücker, J., Umann, B., Sellegri, K., O'Dowd, C. D., and Viisanen, Y.: SO_2 oxidation products other than H_2SO_4 as a trigger of new particle formation – Part 2: Comparison of ambient and laboratory measurements, and atmospheric implications, Atmos. Chem. Phys. Discuss., 8, 9673–9695, 2008, http://www.atmos-chem-phys-discuss.net/8/9673/2008/.

Lee, S.-H. Reeves, J. M., Wilson, J. C., Hunton, D. E., Viggiano, A. A., Miller, T. M., Ballenthin, J. O., and Lait, L. R.: Particle formation by ion nucleation in the upper troposphere and lower stratosphere, Science, 301, 1886–1889, 2003.

Lovejoy, E.R., Curtius, J., and Froyd, K.D.: Atmospheric ion-induced nucleation of sulphuric acid and water, J. Geophys. Res., 109, doi:10.1029/2003JD004460, 2004.

Mäkelä, J. M., Jokinen, V., and Kulmala, M.: Small ion mobilities during particle formation from irradiated SO_2 in humid air, J. Aerosol Sci., 26, Suppl. 1, S333–S334, 1995.

McMurry, P. H. and Eisele, F. L.: Preface to topical collection on new particle formation in Atlanta, J. Geophys. Res., 110, D22S01, doi:10.1029/2005JD006644, 2005.

Mirabel, P. and Clavelin, J. L.: Experimental study of nucleation in binary mixtures: The nitric acid-water and sulphuric acid-water systems, J. Chem. Phys., 68, 5020–5027, 1978.

Napari, I., Noppel, M., Vehkamäki, H., and Kulmala, M.: Parameterization of ternary nucleation rates for H_2SO_4-NH_3-H_2O vapors, J. Geophys. Res., 107, D19, 4381, doi:10.1029/2002JD002132, 2002.

National Institute for Standard Technology (NIST) Chemistry Web Book, NIST Standard Reference Database Number 69, Release (http://webbook.nist.gov/chemistry/), June 2005.

Nowak, J. B., Newman, J. A., Kozai, K., Huey, L. G., Tanner, D. J., Holloway, J. S., Ryerson, T. B., Frost, G. L., McKeen, S. A., and Fehsenfeld, F. C.: A chemical ionization mass spectrometry technique for airborne measurements of ammonia, J. Geophys. Res., 11, D10S02, doi:10.1029/2006JD007589, 2007.

Reiss, H., Margolese, D. I., and Schelling, F. J.: Experimental study of nucleation in vapor mixtures of sulphuric acid and water, J. Colloid Interface Sci., 56, 511–526, 1976.

Seinfeld, J. H. and Pandis, S. N.: Atmospheric chemistry and physics: from air pollution to climate change, Wiley, New York, 545–595, 1997.

Sihto S.-L., Kulmala, M., Kerminen, V.-M., Dal Maso, M., Petäjä, T., Riipinen, L., Korhonen, H., Arnold, F., Jason, R., Boy, M., Laaksonen, A., and Lehtinen, K. E. J.: Atmospheric sulphuric acid and aerosolparticle formation: implications from atmospheric measurements for nucleation and early growth mechanisms, Atmos. Chem. Phys., 6, 4079–4091, 2006, http://www.atmos-chem-phys.net/6/4079/2006/.

Strey, R. and Viisanen, Y.: Measurement of the molecular content

of binary nuclei: use of the nucleation rate surface for ethanol-hexanol, J. Chem. Phys., 99, 4693–4704, 1993.

Svenningsson, B., Arneth, A., Hayward, S., Holst, T., Massling, A., Swietlicki, E., Hirsikko, A., Junninen, H., Riipinen, I., Vana, M., Dal Maso, M., Hussein, T., and Kulmala, M.: Aerosol particle formation events and analysis of high growth rates observed above a subarctic wetlandforest mosaic, Tellus B, 60, 353–364, 2008.

Vehkamäki, H., Kulmala, M., Napari, I., Lehtinen, K. E. J., Timmreck, C., Noppel, M., and Laaksonen, A.: An improved parameterization for sulphuric acid-water nucleation rates for tropospheric and stratospheric conditions, J. Geophys. Res., 107, D22, 4622, doi:10.1029/2002JD002184, 2002.

Viggiano, A. A., Seeley, J. V., Mundis, P. L., Williamson, J. S., and Morris, R. A.: Rate constants for the reactions of $XO_3^-(H_2O)_n$ (X = C, HC, and N) and $NO_3^-(HNO_3)_n$ with H_2SO_4: implications for atmospheric detection of H_2SO_4, J. Phys. Chem. A, 101, 8275–8278, 1997.

Viisanen, Y., Kulmala, M., and Laaksonen, A.: Experiments on gas-liquid nucleation of sulphuric acid and water, J. Chem. Phys., 107, 920–926, 1997.

Weber, R. J., Marti, J. J., McMurry, P. H., Eisele, F. L., Tanner, D. J., and Jefferson, A.: Measured atmospheric new particle formation rates: implications for nucleation mechanisms, Chem. Eng. Commun., 151, 53–64, 1996.

Winkler, P. M., Steiner, G., Vrtala, A., Vehkamäki, H., Noppel, M., Lehtinen, K. E. J., Reischl, G. P., Wagner, P. E., and Kulmala, M.: Heterogeneous nucleation experiments bridging scale from molecular ion clusters to nanoparticles, Science, 319, 1374–1377, 2008.

Wyslouzil, B. E., Seinfeld, J. H., Flagan, R. C., and Okuyama, K.: Binary nucleation in acid-water systems. II. Sulphuric acid-water and a comparison with methanesulphonic acid-water, J. Chem. Phys., 94, 6842–6850, 1991a.

Wyslouzil, B. E., Seinfeld, J. H., Flagan, R. C., and Okuyama, K.: Binary nucleation in acid-water systems, I. Methanesulfonic acid-water, J. Chem. Phys., 94, 6827–6841, 1991b.

Yu, F., Turco, R. P., Kärcher, B., and Schröeder, F. P.: On the mechanisms controlling the formation and properties of volatile particles in aircraft wakes, Geophys. Res. Lett., 25, 3839–3842, 1998.

Yu, F.: Binary H_2SO_4-H_2O homogeneous nucleation based kinetic quasi-unary nucleation mode: Look-up tables, J. Geophys. Res., 111, D04201, doi:10.1029/2005JD006358, 2006.

Zhang, R., Suh, I., Zhao, J., Zhang, D., Fortner, E. C., Tie, X., Monila, L. T., and Monila, M. J.: Atmospheric new particle formation enhanced by organic acids, Science, 304, 1487–1490, 2004.